Stochastic flux freezing and magnetic dynamo

Gregory L. Eyink

Stochastic flux-freezing and magnetic dynamo

Gregory L. Eyink

Department of Applied Mathematics & Statistics
and Department of Physics & Astronomy
The Johns Hopkins University, USA
(Dated: March 17, 2011)

Magnetic flux-conservation in turbulent plasmas at high magnetic Reynolds numbers is argued neither to hold in the conventional sense nor to be entirely broken, but instead to be valid in a novel statistical sense associated to the "spontaneous stochasticity" of Lagrangian particle trajectories. The latter phenomenon is due to the explosive separation of particles undergoing turbulent Richardson diffusion, which leads to a breakdown of Laplacian determinism for classical dynamics. Empirical evidence is presented for spontaneous stochasticity, including new numerical results. A Lagrangian path-integral approach is then exploited to establish stochastic flux-freezing for resistive hydromagnetic equations and to argue, based on the properties of Richardson diffusion, that flux-conservation must remain stochastic at infinite magnetic Reynolds number. An important application of these results is the kinematic, fluctuation dynamo in non-helical, incompressible turbulence at magnetic Prandtl number (Pr_m) equal to unity. Numerical results on the Lagrangian dynamo mechanisms by a stochastic particle method demonstrate a strong similarity between the $Pr_m = 1$ and $Pr_m = 0$ dynamos. Stochasticity of field-line motion is an essential ingredient of both. Some consequences for nonlinear magnetohydrodynamic turbulence, dynamo and reconnection are finally briefly considered.

I. INTRODUCTION

Hannes Alfvén in a seminal paper in 1942 introduced the notion of flux-freezing in magnetohydrodynamic plasmas at infinite conductivity, noting that "every motion (perpendicular to the field) of the liquid in relation to the lines of force is forbidden because it would give infinite eddy currents" [1]. In the years since, the property of flux-conservation has become a powerful tool in the analysis of many near-ideal plasma phenomena. For example, in his excellent monograph [2], Kulsrud states that "The most important property of an ideal plasma is flux-freezing", before proceeding to illustrate its many applications. Of course, physical plasmas in the laboratory and in astrophysics are subject to various forms of non-ideality, including Spitzer resistivity, ambipolar diffusion, etc. The general assumption in the field of plasma physics is that as long as such non-ideality is sufficiently "small", then flux-freezing will hold in an approximate sense. For example, the usual quantitative estimate is well expressed in this quote from Kulsrud's monograph, Ch.13, on magnetic reconnection:

> "Flux freezing is a very strong constraint on the behavior of magnetic fields in astrophysics. As we show in chapter 3, this implies that lines do not break and their topology is preserved. The condition for flux freezing can be formulated as follows: In a time t, a line of force can slip through the plasma a distance

$$\ell = \sqrt{\frac{\eta c t}{4\pi}}. \qquad (1)$$

> If this distance ℓ is small compared to δ, the

scale of interest, then flux freezing holds to a good degree of approximation."

We shall argue that these commonplace ideas on flux-freezing are wrong. They contain an implicit assumption that the plasma fluid remains smooth and laminar for very small non-ideality. The quantitative estimate that field-lines slip through a resistive plasma only a diffusive distance $\propto \sqrt{\eta t}$ in time t is incorrect—by many orders of magnitude—in a turbulent plasma. Since laminar flow at very high kinetic and magnetic Reynolds is unstable to development of turbulence, flux-conservation in the conventional sense must be the exception rather than the rule in astrophysical plasmas. Indeed, we shall show that the standard views on flux-freezing *must* be incorrect, because the very notion of a Lagrangian fluid particle trajectory breaks down in turbulent flow with a spatially "rough" velocity field (i.e. with a power-law kinetic energy spectrum similar to that of Kolmogorov). Recent research has discovered a novel phenomenon of "spontaneous stochasticity", according to which fluid particle trajectories are intrinsically random in high-Reynolds-number turbulence [3–8]. This surprising phenomenon is a long overlooked consequence of the fluid-dynamical effect of Richardson two-particle turbulent dispersion [9]. Because of spontaneous stochasticity, it makes no sense to assume that a field line follows "the" plasma fluid element, because there are infinitely many distinct fluid trajectories starting from the same point! But it is also not true that flux-freezing is completely broken. We shall argue below that magnetic flux-conservation remains valid in the ideal limit of high Reynolds numbers, but in a novel stochastic sense associated with the intrinsic stochasticity of the Lagrangian particle trajectories.

A correct formulation of flux-freezing is fundamental to understand a number of important astrophysical processes, such as turbulent dynamo and reconnection. In previous work [10, 11] we have shown how stochastic flux-freezing is involved in the small-scale "fluctuation dynamo" for a soluble model problem: magnetic fields advected by the Kazantsev-Kraichnan ensemble of velocity fields that are spatially rough and white-noise in time [12–14]. It is worth noting, by the way, that "spontaneous stochasticity" is a rigorously established phenomenon for this model [3–8]. It was shown that presence of fluctuation dynamo effect at zero magnetic Prandtl number depends crucially on the degree of angular correlation between the infinite number of magnetic field vectors that are simultaneously advected by turbulence to the same spatial point [10, 11].

Here we shall make a similar study for kinematic dynamo in non-helical, hydrodynamic turbulence, by a Lagrangian numerical method that employs data from a high-Reynolds-number turbulent flow archived online [15, 16]. We present results for unit magnetic Prandtl number which demonstrate—and quantify—the effect of Richardson diffusion and stochastic flux-freezing on the small-scale turbulent dynamo. We find, in fact, remarkable similarities between the Lagrangian mechanisms of small-scale dynamo in hydrodynamic turbulence at unit Prandtl number and in the Kazantsev model at zero Prandtl number. Previous numerical studies [17, 18] have instead found a close similarity of the unit Prandtl-number fluctuation dynamo with the solution of the Kazantsev model at *infinite* Prandtl-number, observing, in particular, the "Kazantsev spectrum" $k^{3/2}$ of magnetic energy at high wavenumbers. Our new results at much higher Reynolds numbers show that the inertial-range phenomenon of Richardson diffusion strongly affects the exponential growth rate of magnetic energy in the kinematic regime. However, stochastic flux-freezing is not a property of kinematic dynamo only but will hold also for fully nonlinear magnetohydrodynamic (MHD) turbulence and have important implications there for magnetic dynamo and reconnection.

The detailed contents of this paper are as follows: In the following section II we shall briefly review the phenomenon of "spontaneous stochasticity", both its theoretical bases and its present confirmation from simulations and experiments. We aso present new numerical results of our own which support the essential predictions. In Section III we discuss stochastic flux-freezing. We begin with a demonstration of the stochastic flux-conservation properties of resistive MHD, which are novel results themselves. We employ Lagrangian path-integral methods that provide good physical insight. We then discuss the ideal case, via zero-resistivity and other limits. In section IV we employ the new results to analyze the turbulent kinematic dynamo. After discussing the Lagrangian theory of dynamo, we present our numerical results and their comparison with analytical results for the Kazantsev model at zero Prandtl number and

with previous numerical studies. In section V we briefly discuss some implications and open problems for nonlinear MHD turbulence and section VI contains our final discussion. An Appendix sketches the derivation of the path-integral formulas used in the main text.

II. RICHARDSON DIFFUSION AND SPONTANEOUS STOCHASTICITY

A. Richardson 2-particle dispersion

We briefly review Richardson's theory [9] of 2-particle or relative turbulent dispersion, emphasizing perspectives of recent research. The object of Richardson's study was the separation $\Delta\mathbf{x}(t) = \mathbf{x}_1(t) - \mathbf{x}_2(t)$ between a pair of passive Lagrangian tracer particles in a turbulent flow, such as ash particles in a volcanic plume. Richardson's approach was semi-empirical, inferring from data that there is a scale-dependent diffusivity coefficient

$$K(\ell) \sim K_0 \ell^{4/3}. \qquad (1)$$

Richardson proposed further that the probability density function of the separation vector $\boldsymbol{\ell} = \mathbf{x}_1 - \mathbf{x}_2$ would satisfy a diffusion equation

$$\partial_t P(\boldsymbol{\ell}, t) = \frac{\partial}{\partial \ell_i}\left(K(\ell)\frac{\partial P}{\partial \ell_i}(\boldsymbol{\ell}, t)\right). \qquad (2)$$

Finally, Richardson observed that there is an exact similarity solution of his equation given by a stretched-exponential probability density function (PDF), whose form we note here

$$P_*(\boldsymbol{\ell}, t) = \frac{A}{(K_0 t)^{9/2}} \exp\left(-\frac{9\ell^{2/3}}{4K_0 t}\right) \qquad (3)$$

in the physically relevant case of three space dimensions. All solutions of (2) approach this self-similar form asymptotically at long times [19]. Averaging ℓ^2 with respect to the self-similar density (3) yields

$$\langle \ell^2(t) \rangle = \gamma_0 t^3 \qquad (4)$$

with $\gamma_0 = \frac{1144}{81}K_0^3$. This is the famous Richardson t^3-law.

Richardson's work preceded the Kolmogorov 1941 (K41) theory of turbulence, but it was shown by Obukhov [20] to be fully consistent with that theory. This can be seen by a toy calculation in one space dimension. Assume that $\ell(t)$ satisfies the initial-value problem

$$\frac{d}{dt}\ell(t) = \delta u(\ell) = \frac{3}{2}(g_0\varepsilon\ell)^{1/3}, \quad \ell(0) = \ell_0,$$

with velocity increment $\delta u(\ell)$ scaling as in K41 theory, where ε is the mean energy dissipation per unit mass. Separation of variables gives the exact solution

$$\ell(t) = \left[\ell_0^{2/3} + (g_0\varepsilon)^{1/3}t\right]^{3/2}. \qquad (5)$$

If one defines a time $t_0 \equiv \ell_0^{2/3}/(g_0\varepsilon)^{1/3}$ which characterizes the initial separation then, for $t \gg t_0$,

$$\ell^2(t) \sim g_0\varepsilon t^3. \tag{6}$$

For sufficiently long times, the particles "forget" their initial separation and the Richardson law is obtained. The dimensionless parameter g_0 which appears in this form of the t^3-law is usually called the Richardson-Obukhov constant. The physical mechanism of the explosive separation of particles, even faster than ballistic, is the relative advection of the pairs by larger, more energetic eddies as their separation distance increases.

This physics seems relatively simple and benign, but it has extraordinary consequences. As first pointed out in a seminal paper of Bernard, Gawȩdzki, and Kupiainen [3], Richardson's theory implies a breakdown in the usual notion of Laplacian determinism for classical dynamics! This may already be seen in our toy calculation above. If we set $\ell_0 = 0$, then the solution (5) becomes the Richardson law $\ell^2(t) = g_0\varepsilon t^3 > 0$ for all positive times t. Thus, two particles started at the *same* point at time 0 separate to a finite distance at any time $t > 0$. The same oddity may be seen in Richardson's similarity solution (3), which satisfies at initial time $t = 0$

$$P_*(\boldsymbol{\ell}, 0) = \delta^3(\boldsymbol{\ell}).$$

All particles start with separation $\ell(0) = 0$. However, $P_*(\boldsymbol{\ell}, t)$ is a smooth density for $t > 0$, so that $\ell(t) > 0$ with probability one at later times. Richardson's theory thus implies that two particles advected by the fluid velocity $\mathbf{u}(\mathbf{x}, t)$ which start at the *same* initial point $\mathbf{x}_0$

$$\frac{d}{dt}\mathbf{x}(t) = \mathbf{u}(\mathbf{x}(t), t), \quad \mathbf{x}(0) = \mathbf{x}_0$$

can follow different trajectories. This seems to violate the theorem on uniqueness of solutions of initial-value problems for ordinary differential equations (ODE's). However, such theorems assume that the advecting velocity $\mathbf{u}(\mathbf{x}, t)$ is Hölder-Lipschitz continuous in the space variable $\mathbf{x}$

$$|\mathbf{u}(\mathbf{x}_1, t) - \mathbf{u}(\mathbf{x}_2, t)| \leq C|\mathbf{x}_1 - \mathbf{x}_2|^h \tag{7}$$

with exponent $h \geq 1$. A turbulent velocity field in a Kolmogorov inertial range has instead Hölder exponent $h \doteq 1/3$ and the uniqueness theorem need not apply. Our toy calculation above is just the standard textbook example for failure of uniqueness (see Hartman[21], p.2). In that example, for any non-negative "waiting time" $\tau \geq 0$

$$\ell(t) = (g_0\varepsilon)^{1/2}(t - \tau)_+^{3/2}$$

is a solution of the initial-value problem with $\ell_0 = 0$. (Here $(x)_+ = x$ for $x > 0$ and $= 0$ otherwise.)

The above considerations may seem fairly technical and mathematical. It has been shown, however, that this breakdown in uniqueness of trajectories can appear

in various physical limits for turbulent advection. Even more remarkably, the solutions of the deterministic classical dynamics become intrinsically stochastic! See the important series of papers [3–5, 7, 8] and see [6] for a very clear and concise review of the subject.

B. High-Reynolds-number limit and spontaneous stochasticity

The easiest way to understand the phenomenon is via the problem of stochastic particle advection,

$$\frac{d}{dt}\widetilde{\mathbf{x}}(t) = \mathbf{u}^\nu(\widetilde{\mathbf{x}}(t), t) + \sqrt{2\kappa}\,\widetilde{\boldsymbol{\eta}}(t), \quad \mathbf{x}(t_0) = \mathbf{x}_0 \tag{8}$$

with advecting velocity perturbed by a Gaussian white-noise $\widetilde{\boldsymbol{\eta}}(t)$ multiplied by $\sqrt{2\kappa}$ and with velocity assumed spatially smooth at subviscous length-scales $\ell < \ell_\nu$, for a finite viscosity ν. The transition probability for a single particle in a fixed (non-random) velocity realization $\mathbf{u}^\nu$ can be written using a "sum-over-histories" approach as a path-integral [3, 22, 23]:

$$G_{\mathbf{u}}^{\nu,\kappa}(\mathbf{x}_f, t_f|\mathbf{x}_0, t_0) = \int_{\mathbf{x}(t_0)=\mathbf{x}_0} \mathcal{D}\mathbf{x}\,\delta^3(\mathbf{x}_f - \mathbf{x}(t_f))$$
$$\times \exp\left(-\frac{1}{4\kappa}\int_{t_0}^t d\tau\,|\dot{\mathbf{x}}(\tau) - \mathbf{u}^\nu(\mathbf{x}(\tau), \tau)|^2\right). \tag{9}$$

Since this formula plays an important role in our analysis, we provide a self-contained derivation in the Appendix. A physical motivation to study such random advection is the problem of the evolution of a passive scalar, such as a temperature field or dye concentration. These fields solve the scalar advection-diffusion equation

$$\partial_t\theta + (\mathbf{u}^\nu \cdot \boldsymbol{\nabla})\theta = \kappa\triangle\theta, \tag{10}$$

with κ the molecular diffusivity. The exact solution of (10) is given by the Feynman-Kac formula [3, 22, 23]:

$$\theta(\mathbf{x}, t) = \int d^3x_0\,\theta(\mathbf{x}_0, t_0)G_{\mathbf{u}}^{\nu,\kappa}(\mathbf{x}_0, t_0|\mathbf{x}, t)$$
$$= \int_{\mathbf{a}(t)=\mathbf{x}} \mathcal{D}\mathbf{a}\,\theta(\mathbf{a}(t_0), t_0)$$
$$\times \exp\left(-\frac{1}{4\kappa}\int_{t_0}^t d\tau\,|\dot{\mathbf{a}}(\tau) - \mathbf{u}^\nu(\mathbf{a}(\tau), \tau)|^2\right) \tag{11}$$

for $t_0 < t$. This corresponds to solving backward in time the stochastic equation

$$\frac{d}{d\tau}\widetilde{\mathbf{a}}(\tau) = \mathbf{u}^\nu(\widetilde{\mathbf{a}}(\tau), \tau) + \sqrt{2\kappa}\,\widetilde{\boldsymbol{\eta}}(\tau)$$

from $\tau = t$ to $\tau = t_0$, with the condition $\widetilde{\mathbf{a}}(t) = \mathbf{x}$. The present value of the scalar field is thus the average, along stochastic Lagrangian paths, of its earlier values.

It naively appears by an application of the Laplace asymptotic method to (9) that the transition probability collapses to a delta-function

$$G_{\mathbf{u}}^{\nu,\kappa}(\mathbf{x}_f, t_f|\mathbf{x}_0, t_0) \to \delta^3(\mathbf{x}_f - \mathbf{x}(t_f)) \tag{12}$$

as $\kappa \to 0$, with $\mathbf{x}(t)$ the solution of the ODE $\dot{\mathbf{x}} = \mathbf{u}(\mathbf{x}, t)$ for initial condition $\mathbf{x}(t_0) = \mathbf{x}_0$. Only for such time-histories is the action vanishing in the exponent of the path-integral. However, it was shown [3–8] that (12) may not hold if simultaneously $\nu \to 0$ (or the Reynolds-number $Re = u_{rms}L/\nu \to \infty$) and if in that limit the velocity field $\mathbf{u}^\nu \to \mathbf{u}$, for a rough (non-smooth, singular) $\mathbf{u}$. In that case, as $\kappa, \nu \to 0$,

$$G_{\mathbf{u}}^{\nu,\kappa}(\mathbf{x}_f, t_f | \mathbf{x}_0, t_0) \to G_{\mathbf{u}}(\mathbf{x}_f, t_f | \mathbf{x}_0, t_0) \qquad (13)$$

for a nontrivial probability density $G_{\mathbf{u}}$. The Lagrangian trajectories can remain random as $\kappa, \nu \to 0$! This phenomenon has been called "spontaneous stochasticity" [5], because of the analogy with spontaneous symmetry-breaking in condensed matter physics and quantum field-theory, where, for example, a ferromagnet may retain a non-vanishing magnetization even in the limit of vanishing external magnetic field. It is important to appreciate, however, that "spontaneous stochasticity" is a very different type of randomness than is usual in turbulence theory, associated to a random ensemble of velocity fields. Instead, the randomness in (13) is for a fixed (non-random) ensemble member $\mathbf{u}$. The limiting distribution consists of time-histories that are all solutions of the same deterministic initial-value problem

$$\dot{\mathbf{x}} = \mathbf{u}(\mathbf{x}, t), \quad \mathbf{x}(t_0) = \mathbf{x}_0. \qquad (14)$$

As is clear from (9), the limiting probability measure is in a certain sense the uniform or equal-weight distribution over all such solutions. We note in passing that Kneser's theorem in the mathematical theory of ODE's implies that, whenever there is more than one such solution, then there is in fact a continuous infinity of solutions (see Hartman [21], section II.4).

The above results have been rigorously established [3–8] for some model problems of turbulent advection, primarily the *Kraichnan model* of advection by a Gaussian random velocity field with zero mean and covariance

$$\langle u_i^\nu(\mathbf{x}, t) u_j^\nu(\mathbf{x}', t') \rangle = [D_0 \delta_{ij} - S_{ij}^\nu(\mathbf{x} - \mathbf{x}')]\delta(t - t').$$

The velocity fields are temporal white-noise and spatially rough for $\ell_\nu < r < L_u$, with a Hölder exponent $0 < h < 1$, but smooth for $r < \ell_\nu$. We discuss the model only for incompressible flow, in which case

$$S_{ij}^\nu(\mathbf{r}) = \begin{cases} 2D_1[(1+h)\delta_{ij} - h\hat{r}_i\hat{r}_j]r^{2h}, & \ell_\nu \ll r \ll L_u, \\ 2D_1\ell_\nu^{2h-2}[2\delta_{ij} - \hat{r}_i\hat{r}_j]r^2, & r \ll \ell_\nu. \end{cases} \qquad (15)$$

The velocity realizations $\mathbf{u}^\nu(\mathbf{x}, t)$ are divergence-free and Hölder continuous with exponent h for $\nu \equiv D_1\ell_\nu^{2h} \to 0$. The kinetic energy spectra are power-laws k^{-n} for the "inertial range" $1/L_u \ll k \ll 1/\ell_\nu$, with $n = 1 + 2h$ and thus $1 < n < 3$. The key feature which makes this model analytically tractable is the Markovian property in time, which leads to the exact validity of Richardson's 2-particle diffusion equation in the form

$$\partial_t P(\mathbf{r}, t) = \frac{\partial}{\partial r_i}\left(S_{ij}^\nu(\mathbf{r})\frac{\partial P}{\partial r_j}(\mathbf{r}, t)\right) + 2\kappa \triangle_r P(\mathbf{r}, t), \quad (16)$$

with $\mathbf{r} = \mathbf{x}_1 - \mathbf{x}_2$. Note that Richardson's original equation is obtained for $h = 2/3$ rather than the Kolmogorov value $h = 1/3$, a peculiarity of the white-noise approximation. Multiplying (16) by $r_k r_\ell$ and integrating over $\mathbf{r}$ leads to

$$\frac{d}{dt}\langle r_k(t)r_\ell(t)\rangle = 2\langle S_{k\ell}^\nu(\mathbf{r}(t))\rangle + 4\kappa\delta_{k\ell} \qquad (17)$$

An analysis of (16) and (17), for the ensemble of particles which are all started at the same point ($r_0 = 0$) at $t = 0$, leads to the results below. Some of these appear to be new in detail.

For $Pr \equiv \frac{\nu}{\kappa} < 1$, the dispersion is that of two independent Brownian motions in three space dimensions

$$\langle r^2(t)\rangle \sim 12\kappa t \qquad (18)$$

for short times $t \ll t_\kappa = \frac{\ell_\kappa^2}{\kappa}$ with $\ell_\kappa^2 = \left(\frac{\kappa}{D_1}\right)^{1/h} = \ell_\nu^2/(Pr)^{1/h}$, but of Richardson-type

$$\langle r^2(t)\rangle \sim g_h(D_1 t)^{1/(1-h)} \qquad (19)$$

for longer times $t_\kappa \ll t \ll t_L = L^{2(1-h)}/D_1$, with g_h a constant independent of κ. For $Pr > 1$, the behavior is a bit more complex. The result (18) still holds at very short times $t \ll t_\nu \equiv \ell_\nu^2/\nu$, but at large Prandtl numbers there is an intermediate range of exponential growth

$$\langle r^2(t)\rangle \propto \kappa t_\nu e^{2\lambda_\nu t} \qquad (20)$$

for $t_\nu \ll t \ll \ln(Pr)t_\nu$. Here $\lambda_\nu = 10t_\nu^{-1}$ is the generalized Lyapunov exponent (of 2nd-order) for the smooth advecting velocity field [24]. The dispersion at longer times again follows the Richardson law (19). In either case, the Richardson law is valid once $\langle r^2(t)\rangle \gtrsim \max\{\ell_\kappa^2, \ell_\nu^2\}$ and thus holds for arbitrarily small times $t > 0$ in the limit as $\nu, \kappa \to 0$.

A non-vanishing dispersion implies that the Lagrangian trajectories must stay random in the limit. Although the diffusion equation (16) has been averaged over velocity realizations $\mathbf{u}$, it must be the case that $P_{\mathbf{u}}(\mathbf{r}, t|\mathbf{0}, 0) \neq \delta^3(\mathbf{r})$ for $t > 0$ and for a set of $\mathbf{u}$ with nonzero probability, or otherwise the average over $\mathbf{u}$ would also be a delta-function! The physical mechanism of spontaneous stochasticity is clearly the "forgetting" of the length-scales ℓ_κ, ℓ_ν by Richardson diffusion for sufficiently long times, $t \gg t_\kappa, t_\nu$, with those times also vanishing in the limit $\nu, \kappa \to 0$. In the case of incompressible flow, the limiting distribution is completely independent of how the limit is taken. We note in passing that this is *not* true in general for compressible flows and that the possibility for Lagrangian particles to stick as well as to stochastically split allows there to be different limits, depending upon the Prandtl number Pr, in the limit as $\nu, \kappa \to 0$ [4, 8]. However, for incompressible flow the limiting distribution is very universal and robust.

The same limit is obtained for incompressible flow even with $\kappa = 0$ or $Pr = \infty$, if the randomness is intro-

duced through the initial conditions rather than stochastic noise. Consider the solution of the initial-value problem for the Kraichnan ensemble of velocities

$$\frac{d}{dt}\widetilde{\mathbf{x}}(t) = \mathbf{u}^{\nu}(\widetilde{\mathbf{x}}(t), t), \quad \widetilde{\mathbf{x}}(0) = \mathbf{x}_0 + \epsilon\widetilde{\boldsymbol{\rho}}$$

where $\widetilde{\boldsymbol{\rho}}$ is a zero-mean, unit-variance random vector with probability density $Q(\boldsymbol{\rho})$. One may interpret ϵ as the size of error in measuring the initial position of the particle. This corresponds to solving the Richardson diffusion equation (16) with $\kappa = 0$ and initial condition $P^{\epsilon}(\mathbf{r}, 0) = \epsilon^{-3}(Q * Q)(\mathbf{r}/\epsilon)$ so that $P^{\epsilon}(\mathbf{r}, 0) \to \delta^3(\mathbf{r})$ as $\epsilon \to 0$. However, if the limits are taken $\nu \to 0$ first and $\epsilon \to 0$ subsequently, then the solution of the Richardson equation does not degenerate to a delta-function for $t > 0$. This may be seen by solving for the dispersion from eq. (17) with $\kappa = 0$ and $\langle r^2(0) \rangle = 2\epsilon^2$. When $\epsilon < \ell_{\nu}$

$$\langle r^2(t) \rangle \sim 2\epsilon^2 e^{2\lambda_{\nu} t} \tag{21}$$

for times $t \ll t_{\nu} \ln(\ell_{\nu}/\epsilon)$ but for longer times follows the Richardson law (19). When $\ell_{\nu} < \epsilon$ instead, then the short-time behavior is diffusive

$$\langle r^2(t) \rangle \sim 2\epsilon^2 + (const.)D_1\epsilon^{2h}t, \tag{22}$$

for times $t \ll \frac{\epsilon^{2(1-h)}}{D_1}$. Dispersion for such a "random cloud" of initial positions was first considered by Batchelor [25, 26], who obtained instead ballistic growth $\propto t^2$ for hydrodynamic turbulence. The diffusive result above is an artefact of the white-in-time velocity. At times $t \gg \frac{\epsilon^{2(1-h)}}{D_1}$ the Richardson law (19) holds. As in the previous cases, the Richardson law holds for any time $t > 0$ if $\nu, \epsilon \to 0$ with ϵ vanishing slower than $\ell_{\nu}e^{-O(D_1/\ell_{\nu}^{2(1-h)})}$.

As this last discussion should make clear, the phenomenon of "spontaneous stochasticity" is not especially connected with the random perturbation of the motion equations in (8). Instead it is the advection of the particle by a rough velocity field and the "forgetting" of the initial separations which makes the Lagrangian particle motions intrinsically stochastic. Spontaneous stochasticity should not be confused with "chaos", as that term is used in dynamical systems theory [5, 6]. For chaotic dynamical systems with a smooth velocity field, one sees only exponential growth of deviations as in eq.(21). Because this result is proportional to ϵ^2, the initial separation is never "forgotten" and, for all times, $\langle r^2(t) \rangle \to 0$ as $\epsilon \to 0$. For chaotic dynamics, any imprecision in the initial data is exponentially magnified, leading to loss of predictability at long enough times. Spontaneous stochasticity corresponds instead to $\lambda_{\nu} = +\infty$. The solution is unpredictable for *all* future times, even with infinitely precise knowledge of the initial conditions! Furthermore, there is nothing special about the initial time and the solution is non-unique (stochastic) at every point of the Lagrangian path.

C. Experimental and numerical results

Our quantitative discussion above has been based upon the original Richardson theory and, in particular, his diffusion equation (16). This equation is exact for the Kraichnan white-in-time velocity ensemble but is only an approximation for hydrodynamic turbulence, where several of its quantitative predictions are known to be incorrect. We have already mentioned the diffusive short-time growth in dispersion for a particle cloud, eq.(22), which is ballistic for fluid turbulence. (Note that the ballistic regime is correctly predicted by Richardson's diffusion equation for a suitably time-dependent eddy diffusion tensor [26, 27].) The diffusion equation (16) holds in the Kraichnan model also for backward-in-time dispersion. However, actual dispersion rates are different forward and backward in time because of the negative skewness of turbulent velocity increments [27, 28]. There is presently no quantitative theory of turbulent dispersion which successfully accounts for all aspects of the phenomenon. It is necessary to stress that the prediction of "spontaneous stochasticity" has more general grounds in the mathematical theory of ODE's and is not dependent upon the diffusion approximation (16). Nevertheless, in the absence of any fully successful, quantitative theory, it is important to develop understanding from numerical simulations and laboratory experiments. We shall here briefly review the empirical studies of turbulent dispersion and the status of Richardson's theory. In particular, we shall present some new numerical results of our own on stochastic particle advection according to eq.(8) for a turbulent velocity field.

We confine our discussion to just some of the latest studies by experiments [29–32] and simulations [33–35] at the highest Reynolds numbers. Athough the t^3-law (4) and the stretched-exponential PDF (3) are probably the most famous predictions of Richardson's theory, even more important for our discussion is the "forgetting" of initial separations. If r_0 is the initial particle separation distance and ε is energy dissipation per mass, then for times much greater than $t_0 \equiv (r_0^2/\varepsilon)^{1/3}$ both $\langle r^2(t) \rangle$ and $P(r, t)$ should become independent of r_0. As we have seen, this is the crucial physical mechanism underlying spontaneous stochasticity. In general, it has proved rather difficult to observe in a completely consistent and convincing way all of these predictions of Richardson's theory.

Experiments of Ott and Mann at maximum Taylor-scale Reynolds number $Re_T = 107$ observed both a t^3 law and the Richardson PDF, but varied r_0 only by a factor of 1.5 around the value $r_0 = 10\ell_{\nu}$ (for $\ell_{\nu} = (\nu^3/\varepsilon)^{1/4}$ the Kolmogorov dissipation length). Thus, they provide no information on collapse independent of r_0. A series of experiments by Bodenschatz and collaborators [30–32] at substantially higher Reynolds numbers up to $Re_T = 815$ fail to see a t^3 law and instead produce results consistent with Batchelor's ballistic t^2 range. However, their smallest achievable value of the initial separation was only about $r_0 = 30\ell_{\nu}$, so that it is arguable that they

need longer times and still higher Reynolds numbers. At their smallest value of r_0 they did observe Richardson's PDF (3) and for $r_0 = 20$–$150\ell_\nu$ they see results roughly consistent with Richardson's predictions for the quantity $\langle r^{2/3}(t)\rangle - r_0^{2/3}$ and also some tendency to collapse independent of r_0 (see Xu et al. [32], Fig. 1).

Numerical simulations of Ishihara and Kaneda [33] at $Re_T = 283$ showed an inertial-range t^3 law for r_0 in a range between 5–$45\ell_\nu$, but no tendency whatsoever for collapse at long times independent of r_0. However, Biferale et al. [34] in a simulation at nearly identical $Re_T = 284$ and with r_0 in a range of 1.2–$19.6\ell_\nu$, see exactly the opposite: only a slight indication of a t^3-law for their smallest separation but a strong tendency to collapse at long times. They also observe Richardson's PDF (3) for $r_0 = 1.2\ell_\nu$. More recently, Sawford et al. [35] have performed simulations with maximum $Re_T = 650$. They find the best evidence yet of Richardson's predictions for the dispersion (see their Fig.4), with a reasonable t^3 range for $r_0 = 4\ell_\nu$. Other values of r_0 in the range of 0.25–$256\ell_\nu$ do not give a convincing t^3-law but do verify a tendency for collapse at long times.

In view of the incomplete verification of Richardson's predictions, we have undertaken our own numerical investigation. Unlike previous works, however, which have nearly all studied deterministic fluid particles with variable initial separations r_0, we have instead studied the problem of stochastic particle advection according to the eq.(8). The velocity field is obtained from a 1024^3 pseudospectral numerical simulation of forced, statistically stationary turbulence at $Re_T = 433$. The flow data is available online at http://turbulence.pha.jhu.edu and fully documented there and in papers [15, 16]. The entire flow history for about one large-eddy turnover time L_u/u' is archived at a time resolution suitable for particle-tracking experiments, with spatial and temporal interpolation implemented within the database. This is very convenient for our purposes, since it permits us to study particle dispersion backward in time as well as forward. As we have discussed above, it is backward dispersion that is most relevant for turbulent mixing.

We have studied two values of the Prandtl number $Pr = \nu/\kappa = 1$ and 0.1. We solved (8) using the simplest Euler-Maruyama scheme and also, for convergence analysis, an explicit, 1.5th-order strong scheme (Kloeden and Platen [36], Section 11.2). We took time discretization $dt = 10^{-3}$, which guaranteed that particles moved a fraction of ℓ_ν under both turbulent advection and Brownian diffusion at each time-step. The velocity field between stored data-points was interpolated by 6th-order Lagrange polynomials in space and piecewise-cubic Hermite polynomials in time. The results were verified to be converged in dt both by comparison with the higher-order method and with the Euler scheme at a halved step size. We evolved $N = 1024$ independent particle realizations starting at the same initial location, giving 523,776 particle pairs, over the whole time range of the database. For forward tracking we started particles at $t_0 = 0$ and for
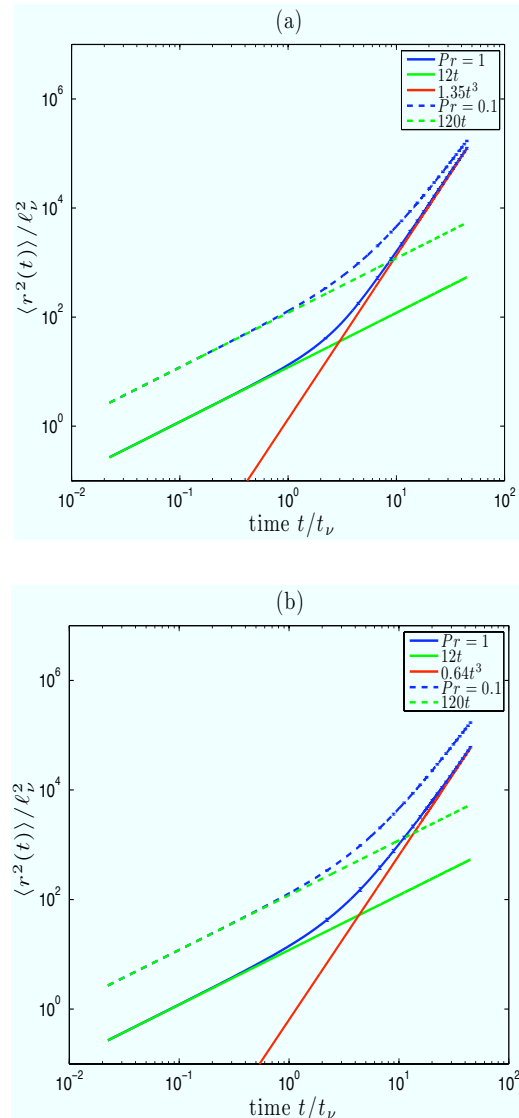

FIG. 1. (Color) Mean dispersion of particle pairs: (a) backward dispersion, (b) forward dispersion. The backward in time results are plotted against $t' = t_f - t$ and all quantities are non-dimensionalized with viscous units (see text). The $Pr = 1$ results are plotted with solid lines (———), $Pr = 0.1$ results with dashed lines (— — —). We color code the lines with blue for raw data (including error bars), green for short-time molecular diffusion, and red for long-time Richardson diffusion.

backward tracking at $t_f = 2.048$ (the final time in the database). We then averaged all results over $S = 512$ initial locations $\mathbf{x}_s$, $s = 1, 2, ..., S$ obtained by choosing 8 independent, uniformly distributed points from each of $4^3 = 64$ subcubes of the whole flow domain.

Our results for particle dispersion are given in Fig.1. We present there a log-log plot of $\langle r^2(t)\rangle$ (normalized

by ℓ_ν^2) versus time t (normalized by $t_\nu = \ell_\nu^2/\nu$). For backward dispersion we take $t \to t' = t_f - t$, to facilitate comparison with the forward-in-time results. We include error bars to show our estimate of the statistical errors. Since the number of pairs of particles being used for each $\mathbf{x}_s$ is quite large, the dominant error in calculating $\langle r^2(t) \rangle$ arises from the average over the S space points. By the central limit theorem, the error is approximated by

$$\delta\langle r^2(t)\rangle \simeq \sqrt{\frac{\mathrm{Var}\left\{\langle r^2(t)\rangle\right\}}{S}} \qquad (23)$$

with the spatial variance

$$\mathrm{Var}\left\{\langle r^2(t)\rangle\right\} \doteq \frac{1}{S-1}\sum_{s=1}^{S}\left|\langle r^2(t)\rangle_{\mathbf{x}_s} - \langle r^2(t)\rangle\right|^2, \quad (24)$$

where $\langle r^2(t)\rangle_{\mathbf{x}_s}$ is the dispersion for the initial particle position $\mathbf{x}_s$. The relative error estimated from (23) is for all times less than 8%. The maximum relative error occurs around $t = 5$ for the forward case and $t = 10$ for the backward case. For larger times the errors are in the range 3-5% for the forward case and 4-5% for the backward case. The error bars are quite small in the log-log plot and allow clear identification of the scaling regimes.

In the viscous units that we employ, the early-time diffusive separation (18) becomes $\langle r^2(t)\rangle \sim 12t/Pr$. This regime is clearly seen for both backward and forward cases and for both $Pr = 1$ and 0.1. Furthermore, for the unit Prandtl number cases, we see a convincing transition to a t^3-law for $t \gtrsim 1$. This occurs slightly earlier for backward dispersion than for forward. Also, we find that the asymptotic Richardson-Obukhov constant is greater for backward dispersion than for forward, in agreement with earlier results [28]. An average of the local constants $g(t) \equiv d\langle r^2(t)\rangle/d(t^3)$ in the t^3-scaling range gives values of $g_0 = 1.35$ for backward dispersion and $g_0 = 0.64$ for forward dispersion. The latter agrees perfectly with a recent theoretical prediction [37] and both are generally consistent with previous values [35]. Pure cube scaling laws with these coefficients are plotted in Fig.1 for comparison with the numerically obtained mean dispersions. The agreement is obviously quite good at long times, especially for the backward case. Even more importantly, the $Pr = 0.1$ dispersions show a very clear trend to approach the same cubic laws at sufficiently large times $t \gg t_\kappa = (\kappa^3/\varepsilon)^{1/4}$ or, in viscous units, $t \gg (Pr)^{-3/4}$. Our Fig.1 thus provides strong evidence of the "forgetting" of the molecular diffusion time-scale t_κ by turbulent Richardson diffusion at long times, which is the essential ingredient of spontaneous stochasticity.

To be completely conclusive, we would need to see collapse of the dispersion curves for different Pr in a range where both show t^3-scaling. We see no clear Richardson t^3 for the $Pr = 0.1$ cases in the time ranges plotted. We cannot continue the time-integration further for two reasons. First, the velocity field from the turbulence archive contains no data for longer times. Second,

the rms dispersion distance $L(t) = \sqrt{\langle r^2(t)\rangle}$ at the final time has reached a value $L(t_f) \doteq 1$, just slightly smaller than the velocity integral length-scale $L_u = 1.376$ for the flow. (This is expected, since t_f is about one large-eddy turnover time.) To integrate further to see a conclusive collapse, we would need a numerical simulation at higher Reynolds numbers and integrated to longer times. However, our confirmation of Richardson diffusion at $Re_T = 433$ using stochastic Lagrangian trajectories is comparable to, or even better than, the results of Sawford et al. [35] at $Re_T = 650$ using deterministic Lagrangian trajectories. (See Fig.4 in that paper). There are two plausible arguments why this should be so. In the first place, using stochastic trajectories, all the particles start at the same point. At the time $t \approx t_\nu$ when $\langle r^2(t) \approx \ell_\nu^2$ (for $Pr = 1$), the particles are not randomly placed in the flow, but have already been experiencing relative advection by different-sized eddies at the onset of the inertial range. Thus, they begin to experience Richardson diffusion at that time. However, using the usual technique of seeding the flow with particles at initial separations $r_0 \doteq \ell_\nu$, one would still need to wait some additional time for the initial configuration to be "forgotten". A second reason is that backward dispersion is faster than forward dispersion, so that the range of t^3 scaling occurs even earlier in that case. The technique of stochastic Lagrangian trajectories appears to be promising in the numerical study of Richardson diffusion.

In order to make a completely convincing case that we are observing Richardson diffusion, we have also numerically calculated the PDF $P(r,t)$ of the particle-separations. Our results for $Pr = 1$ are presented in Fig.2, with the normalization $\int_0^\infty dr\ r^2 P(r,t) = 1$. As has been previously observed [29, 34], Richardson's analytical formula (3) for the long-time PDF of separation distances implies that all the PDF's at different times will collapse when scaled with $L(t) = \sqrt{\langle r^2(t)\rangle}$. In fact, equation (3) is equivalent to

$$L^3(t)P(r,t) = \exp\left[-\alpha\left(\frac{r}{L(t)}\right)^{2/3} + \beta\right]$$

with numerical values

$$\alpha = (1287/8)^{1/3} \doteq 5.4387$$

and

$$\beta = \ln\left(\frac{3}{35}(143)^{3/2}\sqrt{\frac{2}{\pi}}\right) \doteq 4.7617.$$

Thus, Richardson's theory makes a parameter-free prediction that a log-linear plot of $L^3(t)P(r,t)$ versus $(r/L(t))^{2/3}$ should give a straight line with slope $-\alpha$ and y-intercept β. In Fig.2, therefore, we have plotted our PDF's in this way, at three times $t = 22.37, 33.57, 44.79$ all lying in the range of t^3 scaling. We have also plotted the straight line predicted by Richardson's theory. We see that the PDF's scaled in this way collapse very
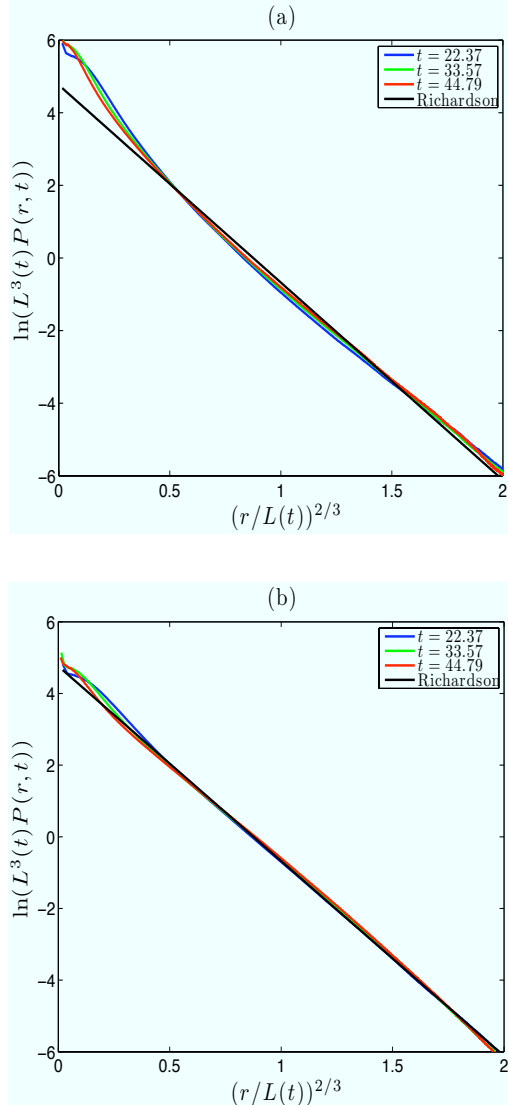
FIG. 2. (Color) Probability densities of pair-separation distances: (a) backward dispersion, (b) forward dispersion. The quantities at different times are normalized by $L(t) = \sqrt{\langle r^2(t)\rangle}$ as shown. We plot densities for three different times in the t^3 scaling range, with blue for $t = 22.37$, green for $t = 33.57$, and red for $t = 44.79$. In the backward case these times correspond to $t' = t_f - t$. The solid black line gives Richardson's analytical prediction for the density (see text).

nicely. Furthermore, except for some deviation at small r in the backward dispersion case, they very closely agree with the predictions of Richardson's theory.

III. STOCHASTIC FLUX-FREEZING

The standard views on flux-freezing in high-conductivity plasmas are inconsistent with the phenomenon of spontaneous stochasticity. It is nearly ubiquitously argued that flux-freezing should hold better as magnetic diffusivity $\lambda \rightarrow 0$. However, high magnetic Reynolds numbers are usually associated also with high kinetic Reynolds numbers. If kinematic viscosity $\nu \rightarrow 0$ simultaneously with the resistivity and if the plasma becomes turbulent, then Lagrangian trajectories will no longer be unique. Which fluid trajectory shall a magnetic field line follow if there are infinitely many such trajectories? This is the paradox of flux-freezing.

As we shall argue below, a form of flux-freezing *does* survive at small resistivities and viscosities, but in a novel stochastic sense. Before we make this argument, however, we shall first discuss the related subject of flux-freezing properties of resistive hydromagnetics.

A. Resistive hydromagnetics

In this subsection we shall discuss magnetic fields that satisfy the resistive induction equation

$$\partial_t \mathbf{B} = \boldsymbol{\nabla} \times (\mathbf{u} \times \mathbf{B} - \lambda \boldsymbol{\nabla} \times \mathbf{B}), \qquad (25)$$

with $\lambda = \eta c/4\pi$ the magnetic diffusivity. It is important to stress that our analysis here applies to a very general velocity field $\mathbf{u}$. It may be incompressible or compressible. It may be externally prescribed or it may satisfy a dynamical equation that contains $\mathbf{B}$ itself. For example, $\mathbf{u}$ may be the plasma velocity that obeys the standard magnetohydrodynamic momentum equation or it may be taken to be $\mathbf{u}_e = \mathbf{u} - \frac{c}{4\pi en} \boldsymbol{\nabla} \times \mathbf{B}$, the electron fluid velocity in Hall magnetohydrodynamics [38]. Our only assumption in this section shall be that $\mathbf{u}$ is a smooth vector field.

A priori there is no obvious way how to describe magnetic-line motion for non-ideal plasmas. One approach that has been widely employed in discussions of magnetic reconnection [39] (or Kuslrud [2], Section 3.4) is to introduce a "slip velocity" $\Delta\mathbf{u} = \mathbf{B} \times (\lambda \boldsymbol{\nabla} \times \mathbf{B})/B^2$. In that case, one may attempt to introduce an "effective velocity" $\mathbf{u}_* = \mathbf{u} + \Delta\mathbf{u}$ of the field lines. Unfortunately, this approach is not generally successful because $(\Delta\mathbf{u}) \times \mathbf{B} = -\lambda \boldsymbol{\nabla} \times \mathbf{B}$ if and only if $\mathbf{B} \cdot \mathbf{E} = 0$ (or $\mathbf{B} \cdot \mathbf{J} = 0$ for Ohmic non-ideality). As has been emphasized [40–42], no effective-velocity approach is satisfactory for discussions of three-dimensional magnetic reconnection. In fact, those authors show that, even if the non-ideality is spatially localized, there generally exists *no* smooth velocity field $\mathbf{u}_*$ whatsoever such that $\partial_t \mathbf{B} = \boldsymbol{\nabla} \times (\mathbf{u}_* \times \mathbf{B})$ for a non-ideal plasma.

For magnetic fields that obey (25), however, there is a natural and consistent way to describe line-motion as a process of *stochastic advection*. Such approaches have

already been employed for some time in discussion of kinematic magnetic dynamos, at least for incompressible velocity fields [43, 44]. Recently, we gave a rigorous proof of stochastic flux-conservation properties for nonlinear hydromagnetic models using mathematical methods of stochastic analysis [45]. We shall present here a more physical demonstration of these results using path-integral methods which, also, extends their validity to compressible fluid models.

To begin, we note that the induction equation (25) may be rewritten as

$$\partial_t \mathbf{B} + (\mathbf{u} \cdot \boldsymbol{\nabla}) \mathbf{B} = (\mathbf{B} \cdot \boldsymbol{\nabla}) \mathbf{u} - \mathbf{B}(\boldsymbol{\nabla} \cdot \mathbf{u}) + \lambda \triangle \mathbf{B}. \quad (26)$$

In this form it is the same as the scalar advection equation (10), except for the additional two terms on the righthand side. The path-integral formula (11) for the scalar solution may thus be easily adapted to this situation. The solution of (26) with initial condition $\mathbf{B}(t_0) = \mathbf{B}_0$ is given by the "sum-over-histories" formula

$$\mathbf{B}(\mathbf{x}, t) = \int_{\mathbf{a}(t) = \mathbf{x}} \mathcal{D}\mathbf{a} \, \mathbf{B}_0(\mathbf{a}(t_0)) \cdot \mathcal{J}(\mathbf{a}, t)$$
$$\times \exp\left(-\frac{1}{4\lambda} \int_{t_0}^t d\tau \, |\dot{\mathbf{a}}(\tau) - \mathbf{u}^\nu(\mathbf{a}(\tau), \tau)|^2\right) \quad (27)$$

where $\mathcal{J}(\mathbf{a}, \tau)$ is a 3×3 matrix and $\mathbf{B}$ is interpreted as a 3-dimensional row vector. Then $\mathcal{J}$ satisfies the following ODE along the trajectory $\mathbf{a}(\tau)$:

$$\frac{d}{d\tau} \mathcal{J}(\mathbf{a}, \tau) = \mathcal{J}(\mathbf{a}, \tau) \boldsymbol{\nabla}_x \mathbf{u}(\mathbf{a}(\tau), \tau)$$
$$- \mathcal{J}(\mathbf{a}, \tau)(\boldsymbol{\nabla}_x \cdot \mathbf{u})(\mathbf{a}(\tau), \tau), \quad (28)$$

with initial condition $\mathcal{J}(\mathbf{a}, t_0) = \mathbf{I}$. It is easy to check by taking the time-derivative of (27) and by using (28) that the induction eq.(26) is satisfied. Just as for the scalar problem, the condition $\mathbf{a}(t) = \mathbf{x}$ on the path-integral trajectories implies that they correspond to solutions of the stochastic equation

$$\frac{d}{d\tau} \widetilde{\mathbf{a}}(\tau) = \mathbf{u}(\widetilde{\mathbf{a}}, \tau) + \sqrt{2\lambda} \, \widetilde{\boldsymbol{\eta}}(\tau), \quad \widetilde{\mathbf{a}}(t) = \mathbf{x} \quad (29)$$

integrated backward in time from $\tau = t$ to $\tau = t_0$.

However, the stochastic equation (29) may also be integrated forward in time from $\tau = t_0$ to $\tau = t$. In that case, the same ensemble of trajectories may be obtained by considering only those particles with initial locations carefully selected to arrive at $\mathbf{x}$ at time t, for a given realization of the white-noise $\widetilde{\boldsymbol{\eta}}(t)$. With a slight change of notation, we may characterize this ensemble of time-histories as those $\widetilde{\mathbf{x}}(\tau)$ which solve

$$\begin{cases} \frac{d}{d\tau} \widetilde{\mathbf{x}}(\mathbf{a}, \tau) = \mathbf{u}(\widetilde{\mathbf{x}}(\mathbf{a}, \tau), \tau) + \sqrt{2\lambda} \, \widetilde{\boldsymbol{\eta}}(\tau), \ \tau > t_0 \\ \widetilde{\mathbf{x}}(\mathbf{a}, t_0) = \mathbf{a} \end{cases} \quad (30)$$

such that the inverse map $\widetilde{\mathbf{a}}(\mathbf{x}, \tau)$ to $\widetilde{\mathbf{x}}(\mathbf{a}, \tau)$ specifies the starting point by $\mathbf{a} = \widetilde{\mathbf{a}}(\mathbf{x}, t)$. Notice that (30) is a stochastic generalization of the usual equation for a Lagrangian flow map $\widetilde{\mathbf{x}}(\mathbf{a}, t)$ of a particle with initial "label"

$\mathbf{a}$ and that $\widetilde{\mathbf{a}}(\mathbf{x}, \tau)$ is the "back-to-labels" map. It is easy to show furthermore by applying $\boldsymbol{\nabla}_a$ to (30) that

$$\widetilde{\mathcal{J}}(\mathbf{a}, t) \equiv \frac{1}{\det\left(\boldsymbol{\nabla}_a \widetilde{\mathbf{x}}(\mathbf{a}, t)\right)} \boldsymbol{\nabla}_a \widetilde{\mathbf{x}}(\mathbf{a}, t). \quad (31)$$

solves equation (28) with initial condition $\widetilde{\mathcal{J}}(\mathbf{a}, t_0) = \mathbf{I}$. It is therefore possible to re-express the path-integral formula (27) as

$$\mathbf{B}(\mathbf{x}, t) = \overline{\frac{1}{\det\left(\boldsymbol{\nabla}_a \widetilde{\mathbf{x}}(\mathbf{a}, t)\right)} \mathbf{B}_0(\mathbf{a}) \cdot \boldsymbol{\nabla}_a \widetilde{\mathbf{x}}(\mathbf{a}, t)|_{\widetilde{\mathbf{a}}(\mathbf{x}, t)}} . \quad (32)$$

The overbar $\overline{}$ represents the average over realizations of the random white noise process $\widetilde{\boldsymbol{\eta}}(t)$ in (30).

We shall call the above result the *stochastic Lundquist formula*, since it is the stochastic generalization of the standard Lundquist formula [46] (or Kulsrud [2], section 4.8). It may be cast into a more familiar form by noting that the determinant that appears there can be interpreted as the ratio of initial and final mass densities [47]:

$$\det\left(\boldsymbol{\nabla}_a \widetilde{\mathbf{x}}(\mathbf{a}, t)\right) = \frac{\rho_0(\mathbf{a})}{\widetilde{\rho}(\widetilde{\mathbf{x}}(\mathbf{a}, t), t)}$$

It follows that the vector field $\widetilde{\mathbf{B}}/\widetilde{\rho}$ is stochastically "frozen-in" and advected along stochastic Lagrangian trajectories, where $\widetilde{\mathbf{B}}$ is defined to be the quantity under the overbar in (32). Notice, therefore, that the average in (32) is not over the frozen-in field $\widetilde{\mathbf{B}}/\widetilde{\rho}$, but rather over the magnetic field $\widetilde{\mathbf{B}}$ itself. This is necessary in order to reproduce the Laplacian term in (26), which has the form $\lambda \triangle \mathbf{B}$ and not $\lambda \triangle (\mathbf{B}/\rho)$.

The use of the stochastic Lundquist formula is illustrated in Fig. 3. The aim is to calculate the magnetic field $\mathbf{B}$ at spacetime point $(\mathbf{x}, t)$. The first step is to generate an ensemble of stochastic Lagrangian trajectories solving (29) backward in time from $\mathbf{x}$ at time t to random locations $\widetilde{\mathbf{a}}(t_0)$ at the initial time t_0. The path-integral formula (27) sums over all such random time-histories. We show in Fig. 3 (top) three stochastic trajectories generated numerically from the turbulence database together with the starting magnetic field vectors $\mathbf{B}_0$, indicated by arrows at the starting locations $\widetilde{\mathbf{a}}(t_0)$. The next step is to transport each of the field vectors in the usual "frozen-in" fashion along the stochastic Lagrangian trajectories to the final spacetime point $(\mathbf{x}, t)$. The result is an ensemble of field vectors $\widetilde{\mathbf{B}}$ at that point, stretched and rotated by the flow. These are illustrated in Fig. 3 (middle) by the collection of three arrows at $(\mathbf{x}, t)$, obtained by transporting the three initial vectors. In the usual deterministic Lundquist formula there would be just one trajectory and one vector $\widetilde{\mathbf{B}}$ at the final point, which would give the desired magnetic field. Now however as the final step one must average over the ensemble of random vectors $\widetilde{\mathbf{B}}$ in order to obtain the resultant magnetic field $\mathbf{B}(\mathbf{x}, t)$. This is illustrated by the black arrow in Fig. 3 (bottom). In contrast to the previous transport step which preserved
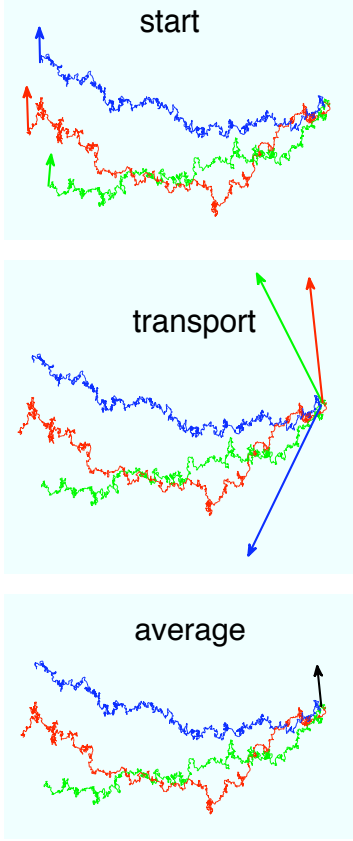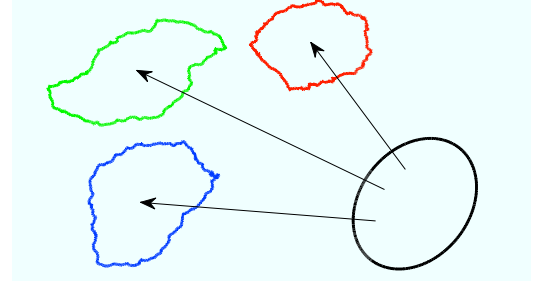
FIG. 4. (Color) Illustration of the stochastic Alfvén theorem. Shown are three members (red, green, blue) of the infinite ensemble of loops obtained by stochastic advection of a loop C (black) at time t backward in time to t_0. The average of the magnetic flux through the ensemble of loops is equal to the magnetic flux through C.

FIG. 3. (Color) Illustration of the stochastic Lundquist formula. Three stochastic Lagrangian trajectories running backward in time from a common point are shown in red, green, blue. Starting field vectors, represented by correspondingly colored arrows, are transported along the trajectories, stretched and rotated, to the common final point. These are then averaged to give the resultant magnetic field at that point, indicated by the black arrow.

line-topology (in each individual realization), the final averaging step resistively "glues" the transported lines together and changes the magnetic field-line topology.

There is an elegant reformulation of the stochastic Lundquist formula which must be mentioned here, both because of its conceptual simplicity and also because of its potentially greater generality (see next subsection). Consider any smooth, oriented surface S at final time t. Then the formula (32) may integrated in $\mathbf{x}$ over the surface S, with respect to the vector area element $d\mathbf{A}(\mathbf{x}) = d\mathbf{x} \times d\mathbf{x}$, and the ensemble-average and surface-integration interchanged on the righthand side. Because the expression under the overbar is the one that appears in the usual Lundquist formula, the standard multi-variable calculus manipulations convert this into a surface integral over $\widetilde{\mathbf{a}}(S,t)$, the surface S randomly

advected backward in time to the initial time t_0. As before $\widetilde{\mathbf{a}}(\cdot,t) = \widetilde{\mathbf{x}}^{-1}(\cdot,t)$ is the "back-to-label map" for the stochastic forward flow. The result is the following *stochastic Alfvén theorem*

$$\int_S \mathbf{B}(\mathbf{x},t)\cdot d\mathbf{A}(\mathbf{x}) = \overline{\int_{\widetilde{\mathbf{a}}(S,t)} \mathbf{B}_0(\mathbf{a})\cdot d\mathbf{A}(\mathbf{a})} \ , \ \ t > t_0.$$
(33)

This result generalizes a previous theorem [45] to compressible plasmas. Eq.(33) expresses the conservation of magnetic flux on average, as illustrated in Fig. 4. An initial loop C, boundary of the surface S, is shown there in black. This is stochastically advected backward in time to give an infinite ensemble of loops at the initial time t_0. These are represented by the three colored loops. The ensemble-average of the magnetic flux through the collection of loops at the initial time t_0 is equal to the magnetic flux through the loop C at the final time t.

The stochastic Alfvén theorem is an example of what is called a "martingale property" in probability theory. The magnetic flux through each advected loop at the earlier time t_0 is unequal to the magnetic flux through C at time t. Nevertheless, the mean flux remains the same. Note that this result implies an irreversibility or an "arrow of time" since it only holds for backward stochastic advection of loops. Backward-in-time is the causal direction, since the magnetic flux at the present must be obtained as an average of past values and not of future values. If we assumed a "forward martingale" property then we would obtain instead the magnetic induction equation (26) with a *negative* resistivity term $-\lambda \triangle \mathbf{B}$. Note, in fact, that the stochastic Alfvén theorem (backward in time) is mathematically equivalent to the usual resistive induction equation (25) or (26) [45].

B. High-Reynolds-number limit

We now consider the limit of large kinematic and magnetic Reynolds numbers. For simplicity we shall assume that $Pr_m = \nu/\lambda$ remains fixed as $\nu, \lambda \to 0$.

Consider the Feynman-Kac formula (27). By a naive application of the Laplace method, one would assume that the path-integral collapses to a single deterministic trajectory as $\lambda \to 0$, with rms fluctuations of order $(\lambda t)^{1/2}$ for small but nonzero λ. This is precisely the heuristic estimate of line-slippage made by Kulsrud [2] which was quoted in the Introduction. This estimate is rigorously correct if the velocity and magnetic fields are assumed to remain smooth in the limit $\nu, \lambda \to 0$. Thus, the heuristic estimate is correct if the plasma flow remains laminar, but this will be the exception rather than the rule at high Reynolds numbers. In a turbulent flow, the behavior will be quite different. As we can see from our Fig. 1 for incompressible hydrodynamic turbulence, the heuristic estimate is only valid for very short times smaller than the resistive time $t_\lambda = (\lambda^3/\varepsilon)^{1/4}$. At longer times, the rms slip distance of the field lines instead follows the Richardson law $\sim (\varepsilon t^3)^{1/2}$, independent of ν and λ. The quantitative behavior will be different in plasmas with strong magnetic fields, due to the effects of the Lorentz force, as discussed more in section V. However, the qualitative behavior must be the same whenever the advecting velocity is turbulent and spatially rough.

The Feynman-Kac formula (27) is not very well-suited to analyzing the limit of high Reynolds numbers, however, because the velocity-gradients that appear in the definition of the matrix $\mathcal{J}$ diverge in that limit. Likewise, the gradients of the Lagrangian flow map that appear in the definition (31) of $\widetilde{\mathcal{J}}$ are expected to diverge. The integrated form of flux-conservation, the stochastic Alfvén theorem (33), is more likely to remain meaningful in the limit of infinite Reynolds number. The backward-advected loops $\widetilde{\mathbf{a}}^\lambda(C, t)$ at finite values of λ, ν are expected to approach well-defined curves $\widetilde{\mathbf{a}}(C, t)$ as $\lambda \to 0$, which, however, are not rectifiable but fractal [48, 49]. To make mathematical sense of magnetic flux through such fractal loops, we may introduce the vector potential $\mathbf{A}_0 = (\text{curl})^{-1}\mathbf{B}_0$ and rewrite the flux through surface $\widetilde{\mathbf{a}}(S, t)$ as a line-integral around its perimeter $\widetilde{\mathbf{a}}(C, t)$. We may then further transform by change of variables to a line-integral around the original loop C, as:

$$\oint_{\widetilde{\mathbf{a}}(C,t)} \mathbf{A}_0(\mathbf{a}) \cdot d\mathbf{a} = \oint_C \mathbf{A}_0(\widetilde{\mathbf{a}}(\mathbf{x}, t)) \cdot d\widetilde{\mathbf{a}}(\mathbf{x}, t).$$

The integral on the right may be interpreted as a generalized Stieltjes integral, which is well-defined as long as the map $\widetilde{\mathbf{a}}(\mathbf{x}, t)$ is suitably Hölder continuous [50].

It may seem from our arguments to this point that the validity at very high Reynolds numbers of the stochastic flux-freezing result (33) is dependent upon the particular stochastic representation of resistive effects employed in eqs.(30) and (32). However, the same "martingale property" can be obtained in the limit $\nu, \lambda \to 0$ by a different argument that employs only the standard Lagrangian flow [51]. Define the deterministic flow, as usual, by

$$\begin{cases} \frac{d}{d\tau}\mathbf{x}^\nu(\mathbf{a}, \tau) = \mathbf{u}^\nu(\mathbf{x}^\nu(\mathbf{a}, \tau), \tau), & \tau > t_0 \\ \mathbf{x}^\nu(\mathbf{a}, t_0) = \mathbf{a} \end{cases} \quad (34)$$

where the superscript ν is a reminder that the dynamical equation for the advecting velocity field contains a certain viscosity $\nu = (Pr)\lambda$. Correspondingly one defines the inverse map $\mathbf{a}^\nu(\cdot, t) = (\mathbf{x}^\nu)^{-1}(\cdot, t)$. Stochasticity can be introduced by assuming small random perturbations of the loop, taking $C \to C + \epsilon\widetilde{C}$, where $\widetilde{C}$ is a random loop from a well-behaved ensemble [52]. Thus, ϵ can be regarded as the spatial-resolution in determining the precise form of the loop C. We may then argue that, at least for incompressible flow, the ensemble of loops $\widetilde{\mathbf{a}}^\lambda(C, t)$ obtained from stochastic advection in the limit $\lambda \to 0$ coincides with the ensemble of loops obtained from deterministic advection $\mathbf{a}^\nu(C + \epsilon\widetilde{C}, t)$ taking the limits first $\nu, \lambda \to 0$ and then $\epsilon \to 0$. As discussed in the previous section, this is rigorously known to be true for point-particles advected by velocities selected from the Kraichnan white-in-time ensemble [7]. The physical mechanism is just turbulent Richardson diffusion. We therefore conjecture that the same result holds for loops. If this is so, then the double limit

$$\lim_{\epsilon \to 0} \lim_{\nu, \lambda \to 0} \oint_{\mathbf{a}^\nu(C + \epsilon\widetilde{C}, t)} \mathbf{A}_0(\mathbf{a}) \cdot d\mathbf{a}$$

gives precisely the same ensemble of fluxes with the same distribution as in the previous approach. In that case, (33) must again hold in the limit, or, more precisely,

$$\oint_C \mathbf{A}(\mathbf{x}, t) \cdot d\mathbf{x} = \lim_{\epsilon \to 0} \lim_{\nu, \lambda \to 0} \overline{\oint_{\mathbf{a}^\nu(C + \epsilon\widetilde{C}, t)} \mathbf{A}_0(\mathbf{a}) \cdot d\mathbf{a}}, \quad (35)$$

where $\mathbf{A} = \lim_{\nu, \lambda \to 0} \mathbf{A}^\lambda$ and the overbar now indicates average over the ensemble of loop perturbations $\widetilde{C}$. This is a nontrivial result because for an individual loop C

$$\frac{d}{dt} \oint_{\mathbf{x}^\nu(C, t)} \mathbf{A}^\lambda(\mathbf{x}, t) \cdot d\mathbf{x} = -\lambda \oint_{\mathbf{x}^\nu(C, t)} (\boldsymbol{\nabla} \times \mathbf{B}^\lambda)(\mathbf{x}, t) \cdot d\mathbf{x}.$$

Since $\boldsymbol{\nabla} \times \mathbf{B}^\lambda$ diverges in the limit $\nu, \lambda \to 0$, there is no reason to expect that the righthand size vanishes in that limit. This is the standard argument how flux-freezing can be violated in thin current-sheets. It stands to reason that magnetic flux through an individual Lagrangian loop will fluctuate in time and not be conserved. Nevertheless, our arguments lead us to conclude that flux-freezing in turbulent flow is still preserved in the mean sense (35) at infinite Reynolds number.

A scalar resistivity of the form in (25) or (26), in fact, plays no essential role in our arguments. Any microscopic plasma mechanism of "line slippage" will be accelerated by turbulent advection as soon as the lines have separated by a distance of order ℓ_ν, the viscous length. More

realistic mechanisms of line-slippage such as anisotropic resistivity in the Braginski equations [53] (also Kulsrud [2], Ch.8) or the Hall effect often invoked in theories of fast reconnection [54] may all serve the same role. After a very short time the microscopic plasma mechanism of line-slippage, whatever it may be, will be "forgotten" and replaced by turbulent Richardson diffusion.

IV.   TURBULENT MAGNETIC DYNAMO

The stochasticity of flux-freezing plays an essential role in the operation of the turbulent magnetic dynamo. We have already made a detailed analysis of this in the Kazantsev-Kraichnan model of fluctuation kinematic dynamo for a non-helical, incompressible velocity field, with $Rm = \infty$ and $Pr_m = 0$ [10, 11]. Here we shall present a more general study. We first discuss how our path-integral approach relates to the standard Lagrangian formulations of magnetic dynamo [43, 44, 55–59], in a framework that encompasses helical and/or compressible flows and turbulent velocity fields with realistic time-correlations. We focus on the kinematic dynamo here but much of our discussion carries over also to the nonlinear dynamo (which is considered more specifically in section V). We then present numerical results for a particular case, the kinematic fluctuation dynamo in a non-helical, incompressible turbulent velocity field for $Pr_m = 1$, using the same hydrodynamic turbulence database that was employed in our study of Richardson diffusion (section II.C). We compare our results with earlier numerical studies [17, 18, 60, 61] at lower Reynolds number and, also, with our previous analytical results in the Kazantsev-Kraichnan model at $Pr_m = 0$ [11]. As we shall see, spontaneous stochasticity and Richardson diffusion play a very similar role in the fluctuation dynamo for both $Pr_m = 0$ and $Pr_m = 1$.

A.   Lagrangian description of dynamo

The Feynman-Kac formula (27) for the magnetic field may be rewritten as

$$B^i(\mathbf{x}, t) = \int d^3a \, B_0^k(\mathbf{a}) \hat{F}_k^i(\mathbf{a}, t_0 | \mathbf{x}, t; \mathbf{u}) \qquad (36)$$

with the definition

$$\hat{F}_k^i(\mathbf{a}, t_0 | \mathbf{x}, t; \mathbf{u}) = \int_{\boldsymbol{\alpha}(t)=\mathbf{x}} \mathcal{D}\boldsymbol{\alpha} \, \delta^3(\boldsymbol{\alpha}(t_0) - \mathbf{a}) \mathcal{J}_k^i(\boldsymbol{\alpha}, t)$$
$$\times \exp\left(-\frac{1}{4\lambda} \int_{t_0}^{t} d\tau \, |\dot{\boldsymbol{\alpha}}(\tau) - \mathbf{u}^\nu(\boldsymbol{\alpha}(\tau), \tau)|^2\right). \quad (37)$$

This latter quantity is a generalization to a compressible flow of the (Eulerian) magnetic Green's function considered by Lerche [62] and Kraichnan [56], expressed as a Lagrangian path-integral. It completely encodes all the effects of the advecting flow.

A description of the *mean-field dynamo* is obtained if one averages over the ensemble of velocity fields and the random initial conditions of the magnetic field. Assuming that these are statistically independent (which requires that the effects of the Lorenz force be negligible),

$$\langle B^i(\mathbf{x}, t) \rangle = \int d^3a \, \langle B_0^k(\mathbf{a}) \rangle F_k^i(\mathbf{a}, t_0 | \mathbf{x}, t) \qquad (38)$$

with $F_k^i(\mathbf{a}, t_0 | \mathbf{x}, t) \equiv \langle \hat{F}_k^i(\mathbf{a}, t_0 | \mathbf{x}, t) \rangle$ the mean magnetic Green's function. The same result holds without the assumption of kinematic dynamo if the initial magnetic field is non-random and the mean Green's function is defined by a conditional average for fixed $\mathbf{B}_0$ [59]. Of course, in that case the mean Green's function becomes dependent upon the magnetic field. The mean Green's function involves Taylor 1-particle diffusion, or absolute diffusion with respect to a starting point $\mathbf{x}$ at time t, with the stochastic fluid particle moving backward to time t_0. In the case of homogeneous velocity statistics,

$$F_k^i(\boldsymbol{\rho}; t_0, t) \equiv F_k^i(\boldsymbol{\rho}, t_0 | \mathbf{0}, t)$$

becomes a function of the single variable $\boldsymbol{\rho} = \mathbf{a} - \mathbf{x}$. The large-$\rho$ behavior of the mean magnetic Green's function is well-known if the velocity statistics are also isotropic (but reflection non-symmetric), in which case the usual α and β effects of mean-field electrodynamics determine the large-distance decay (see Kraichnan [56], eq.(3.17)). In particular, the mean Green's function is non-negligible only for $\rho = O\left((\beta|t - t_0|)^{1/2}\right)$, with β the eddy-diffusivity of the mean magnetic field. If the magnetic field statistics are also homogeneous, then the mean field $\langle \mathbf{B}(\mathbf{x}, t) \rangle = \langle \mathbf{B}_0 \rangle$ becomes time-independent (no mean-field dynamo), in which case (38) yields the sum-rule

$$\int d^3\rho \, F_k^i(\boldsymbol{\rho}; t_0, t) = \delta_k^i. \qquad (39)$$

The exact Lagrangian formulas for the mean-field electrodynamics coefficients, α, β, etc., that were derived by Moffatt [55] and Kraichnan [56, 57] at infinite conductivity, hold also for positive resistivity within the present stochastic framework [43, 44, 59]. These formulas involve the stochastic displacement field $\widetilde{\boldsymbol{\xi}}(\mathbf{x}, t) = \mathbf{x} - \widetilde{\mathbf{a}}(\mathbf{x}, t)$ of 1-particle turbulent diffusion [63]

As a side remark, we note that the results on the mean Green's function in homogeneous, isotropic turbulence which we reviewed in the text may have limited relevance to the description of astrophysical dynamos and laboratory dynamo experiments. The separation of scales required for the applicability of mean-field electrodynamics often does not occur in practice and large-scale magnetic fields might not be understood without reference to object-specific features, global flow geometry and boundary-conditions. In fact, as a general rule, mean-field dynamo effect requires not just turbulent diffusion of field-lines but also a globally organized motion of magnetic fields. To show this, we present an argument based

on Faraday's law for the mean field

$$\partial_t \langle \mathbf{B} \rangle + \boldsymbol{\nabla} \cdot \boldsymbol{\Sigma} = 0,$$

rewritten as a local conservation law for the magnetic field vector. Here

$$\Sigma^{ij} = \langle u^i B^j - u^j B^i \rangle + \lambda \left(\frac{\partial \langle B^i \rangle}{\partial x_j} - \frac{\partial \langle B^j \rangle}{\partial x_i} \right)$$

represents the spatial flux of the jth component of mean magnetic field in the ith coordinate direction. The space-average of $\langle \mathbf{B}(\mathbf{x}, t) \rangle$ over a volume V can only change in time by a transport of magnetic field lines through its surface ∂V. Furthermore, a simple calculation with Ampere's law $\langle \mathbf{J} \rangle = \frac{1}{4\pi} \boldsymbol{\nabla} \times \langle \mathbf{B} \rangle$ gives

$$\frac{d}{dt} \int \frac{1}{8\pi} |\langle \mathbf{B}(\mathbf{x}, t) \rangle|^2 \, d^3 x = \int \frac{1}{2} \epsilon_{ijk} \langle J^i \rangle \Sigma^{jk} \, d^3 x,$$

where the integral is over all of space. We see that energy in the mean-field $\langle \mathbf{B} \rangle$ grows when the transport of magnetic flux across the closed lines of mean electric current reinforces the Amperian fields induced by those currents (using the righthand rule). We thus see that mean-field dynamo action requires coherent motion of magnetic field lines, coordinated over large spatial scales. Note that very similar ideas are widely used in condensed matter physics to explain, for example, the decay of magnetic flux through a superconducting ring by "phase-slippage" of quantized field lines [64].

Returning to the discussion of small-scale turbulence, we note that a formula for the magnetic correlation function analogous to (38) for the mean field can be derived, under precisely the same assumptions:

$$\langle B^i(\mathbf{x}, t) B^j(\mathbf{x}', t) \rangle = \int d^3 a \int d^3 a' \, \langle B_0^k(\mathbf{a}) B_0^\ell(\mathbf{a}') \rangle \\ \times F_{k\ell}^{ij}(\mathbf{a}, \mathbf{a}', t_0 | \mathbf{x}, \mathbf{x}', t) \quad (40)$$

with[65]

$$F_{k\ell}^{ij}(\mathbf{a}, \mathbf{a}', t_0 | \mathbf{x}, \mathbf{x}', t) = \langle \hat{F}_k^i(\mathbf{a}, t_0 | \mathbf{x}, t) \hat{F}_\ell^j(\mathbf{a}', t_0 | \mathbf{x}, t) \rangle. \quad (41)$$

The behavior of this "two-body" Green's function is determined by the properties of turbulent 2-particle (Richardson) diffusion effects. E.g. setting $\mathbf{x} = \mathbf{x}'$ in the above formula leads to an expression for mean magnetic energy density $\langle B^2(\mathbf{x}, t) \rangle$, which is related to pairs of stochastic Lagrangian trajectories (with independent Brownian motions) that start at points $\mathbf{a}$ and $\mathbf{a}'$ at time t_0 and both end at $\mathbf{x}$ at time t.

Combining (38) and (40) gives a formula for the correlation of the magnetic fluctuations:

$$\langle B^i(\mathbf{x}, t) B^j(\mathbf{x}', t) \rangle - \langle B^i(\mathbf{x}, t) \rangle \langle B^j(\mathbf{x}', t) \rangle$$

$$= \int d^3 a \int d^3 a' \left[\langle B_0^k(\mathbf{a}) B_0^\ell(\mathbf{a}') \rangle - \langle B_0^k(\mathbf{a}) \rangle \langle B_0^\ell(\mathbf{a}') \rangle \right] \\ \times F_{k\ell}^{ij}(\mathbf{a}, \mathbf{a}', t_0 | \mathbf{x}, \mathbf{x}', t)$$

$$+ \int d^3 a \int d^3 a' \, \langle B_0^k(\mathbf{a}) \rangle \langle B_0^\ell(\mathbf{a}') \rangle \\ \times \left[F_{k\ell}^{ij}(\mathbf{a}, \mathbf{a}', t_0 | \mathbf{x}, \mathbf{x}', t) - F_k^i(\mathbf{a}, t_0 | \mathbf{x}, t) F_\ell^j(\mathbf{a}', t_0 | \mathbf{x}, t) \right]. (42)$$

The first term on the righthand side represents *fluctuation dynamo* due to growth of magnetic fluctuations, whereas the second term represents *magnetic induction*, or the generation of magnetic fluctuations from the mean field by random advection. Note that for $|\mathbf{x} - \mathbf{x}'| \gg L_u$, the integral correlation length of the velocity field,

$$F_{k\ell}^{ij}(\mathbf{a}, \mathbf{a}', t_0 | \mathbf{x}, \mathbf{x}', t) \simeq F_k^i(\mathbf{a}, t_0 | \mathbf{x}, t) F_\ell^j(\mathbf{a}', t_0 | \mathbf{x}, t),$$

because the two stochastic particle trajectories become statistically independent. As a consequence, the second magnetic induction term in (42) always goes to zero for $|\mathbf{x} - \mathbf{x}'| \to \infty$. The first term will also vanish in that limit if $\langle B_0^k(\mathbf{a}) B_0^\ell(\mathbf{a}') \rangle - \langle B_0^k(\mathbf{a}) \rangle \langle B_0^\ell(\mathbf{a}') \rangle \to 0$ for $|\mathbf{a} - \mathbf{a}'| \to \infty$ (statistical "clustering" of initial data).

The above formulas simplify in the special case of spatially homogeneous statistics for both the velocity and magnetic fields. In particular, (40) becomes

$$\langle B^i(\mathbf{r}, t) B^j(\mathbf{0}, t) \rangle = \int d^3 \rho \, \langle B_0^k(\boldsymbol{\rho}) B_0^\ell(\mathbf{0}) \rangle \, F_{k\ell}^{ij}(\boldsymbol{\rho}, t_0 | \mathbf{r}, t). \quad (43)$$

with the homogeneous 2-body mean Green's function

$$F_{k\ell}^{ij}(\boldsymbol{\rho}, t_0 | \mathbf{r}, t) \equiv \int d^3 a \, F_{k\ell}^{ij}(\mathbf{a}, \mathbf{a} + \boldsymbol{\rho}, t_0 | \mathbf{x}, \mathbf{x} + \mathbf{r}, t). \quad (44)$$

For $|\mathbf{r}| \gg L_u$,

$$F_{k\ell}^{ij}(\boldsymbol{\rho}, t_0 | \mathbf{r}, t) \simeq \int d^3 a \, F_k^i(\mathbf{a} + \boldsymbol{\rho}; t_0, t) F_\ell^j(\mathbf{a} + \mathbf{r}; t_0, t),$$

and the 2-body Green's function is non-negligible only for $|\boldsymbol{\rho} - \mathbf{r}| = O\left((\beta |t - t_0|)^{1/2}\right)$. Then (39) implies that

$$\lim_{|\mathbf{r}| \to \infty} \int d^3 \rho \, F_{k\ell}^{ij}(\boldsymbol{\rho}, t_0 | \mathbf{r}, t) = \delta_k^i \delta_\ell^j. \quad (45)$$

These properties will be used in our discussion of the numerical results below.

B. Numerical study of kinematic dynamo

We now present a numerical study of small-scale turbulent kinematic dynamo at $Pr_m = 1$. We employ the same database of non-helical, incompressible fluid turbulence that was used in our investigation of Richardson diffusion in section II.C. This might appear to be a poor choice at first sight, since the conventional view [17, 18] is that the kinematic fluctuation dynamo at $Pr_m = 1$ is a phenomenon of sub-viscous scales. For this reason, the previous numerical studies have taken special pains to resolve well the viscous range, at a sacrifice of Reynolds number. For example, the highest resolution 1024^3 simulation of

Haugen et al. [17] had a Taylor-scale Reynolds number $Re_T = 230$ which is nearly half that of the database that we employ, for which $Re_T = 433$ [15, 16]. The previous numerical results seemed to verify the idea that viscous scales played the dominant role; for example, the magnetic energy spectrum in the kinematic regime was found to be peaked at wavenumbers a little higher than the viscous Kolmogorov wavenumber k_ν. See Haugen et al. [17], Fig. 4 and Schekochihin et al.[18], Fig. 22(a). The viscous range is not so well-resolved in the database that we employ, with the grid spacing Δx of the simulation being slightly greater than $2\ell_\nu$. Nevertheless, our study was designed to show the critical role of inertial-range advection to the small-scale turbulent dynamo at high Reynolds numbers and, thus, was forced to sacrifice resolution of the viscous range. Our results will show that both ranges play a critical role at $Pr_m = 1$ and, we will argue, even for Pr_m much larger.

1. Methods

Our Lagrangian numerical approach is based upon the results in section III.A. We construct an ensemble of stochastic particles that solve eq.(29) backward in time from common starting point $\mathbf{x}$. The Feynman-Kac formula (27) then yields

$$B^2(\mathbf{x}, t_f) = \overline{\overline{B_0^i(\widetilde{\mathbf{a}}(t_0)) B_0^j(\widetilde{\mathbf{a}}'(t_0)) \left(\boldsymbol{\mathcal{J}}(\widetilde{\mathbf{a}}, t_f, t_0) \boldsymbol{\mathcal{J}}^\top(\widetilde{\mathbf{a}}', t_f, t_0) \right)_{ij}}},$$

where the double-overline indicates an average over two ensembles of trajectories $\widetilde{\mathbf{a}}(t)$, $\widetilde{\mathbf{a}}'(t)$ with independent realizations of the Brownian noise. The $\boldsymbol{\mathcal{J}}$ matrix satisfies equation (28) for $\boldsymbol{\nabla}_x \cdot \mathbf{u} = 0$:

$$\begin{cases} \frac{d}{dt_f} \boldsymbol{\mathcal{J}}(\widetilde{\mathbf{a}}, t_f, t_0) = \boldsymbol{\mathcal{J}}(\widetilde{\mathbf{a}}, t_f, t_0) \boldsymbol{\nabla}_x \mathbf{u}(\widetilde{\mathbf{a}}(t_f), t_f), \\ \boldsymbol{\mathcal{J}}(\widetilde{\mathbf{a}}, t_0, t_0) = \mathbf{I}. \end{cases}$$

The exact solution of this equation is an anti-time-ordered exponential of the velocity-gradient from t_0 to t_f and we have here indicated explicitly the dependence of $\boldsymbol{\mathcal{J}}$ upon both times. As a matter of fact, it is numerically easier to use the ODE in the initial time t_0

$$\begin{cases} \frac{d}{d\tau} \boldsymbol{\mathcal{J}}(\widetilde{\mathbf{a}}, t_f, \tau) = -\boldsymbol{\nabla}_x \mathbf{u}(\widetilde{\mathbf{a}}(\tau), \tau) \boldsymbol{\mathcal{J}}(\widetilde{\mathbf{a}}, t_f, \tau), \\ \boldsymbol{\mathcal{J}}(\widetilde{\mathbf{a}}, t_f, t_f) = \mathbf{I}, \end{cases} \quad (46)$$

which may be solved backward in time from $\tau = t_f$ to $\tau = t_0$ along with the stochastic equations (29). We then average over an ensemble of initial conditions $\mathbf{B}_0$ (the same for each τ) to obtain the mean magnetic energy

$$\langle B^2(\mathbf{x}, t_f) \rangle_\tau = \overline{\overline{\langle B_0^i(\widetilde{\mathbf{a}}(\tau)) B_0^j(\widetilde{\mathbf{a}}'(\tau)) \rangle \left(\boldsymbol{\mathcal{J}}(\widetilde{\mathbf{a}}, t_f, \tau) \boldsymbol{\mathcal{J}}^\top(\widetilde{\mathbf{a}}', t_f, \tau) \right)_{ij}}}.$$

In effect we are solving for the growth of magnetic field by moving the time τ of the initial conditions backward

rather than advancing t_f forward. Thus, our results below shall be plotted with respect to the difference variable $t = t_f - \tau$. Assuming ergodicity, an average over space

$$\langle B^2(t) \rangle \equiv \frac{1}{V} \int d^3 x \, \langle B^2(\mathbf{x}, t_f) \rangle_\tau$$

is equivalent to an average over an ensemble of velocities. In a statistical steady state, this average should indeed be a function only of the difference variable $t = t_f - \tau$.

To further simplify matters, we take as our initial seed field for the dynamo a spatially uniform magnetic field $\mathbf{B}_0$ which is still random, however, and statistically isotropic. The covariance choice $\langle B_0^i B_0^j \rangle = \frac{1}{3} \delta^{ij}$ implies a magnetic energy initially equal to one. This is not very small, but there is no requirement of small field strength in our kinematic problem. The formula for the mean magnetic energy then factorizes as

$$\langle B^2(\mathbf{x}, t_f) \rangle_\tau = \overline{\overline{\frac{1}{3} \text{tr} \left(\boldsymbol{\mathcal{J}}(\widetilde{\mathbf{a}}, t_f, \tau) \boldsymbol{\mathcal{J}}^\top(\widetilde{\mathbf{a}}', t_f, \tau) \right)}}$$
$$= \frac{1}{3} \text{tr} \left(\bar{\boldsymbol{\mathcal{J}}}(t_f, \tau) \bar{\boldsymbol{\mathcal{J}}}^\top(t_f, \tau) \right), \quad (47)$$

where $\bar{\boldsymbol{\mathcal{J}}}(t_f, \tau) \equiv \overline{\boldsymbol{\mathcal{J}}(\widetilde{\mathbf{a}}, t_f, \tau)}$. Note that $\mathbf{F} = \bar{\boldsymbol{\mathcal{J}}} \bar{\boldsymbol{\mathcal{J}}}^\top$ is a positive-definite, symmetric matrix which formally reduces in the limit of vanishing noise to the usual (left) Cauchy-Green or Finger deformation tensor of continuum mechanics. The initially uniform magnetic field does not stay uniform but develops small-scale fluctuations by an induction effect. There is, in fact, no very precise distinction between "magnetic induction" and "fluctuation dynamo", as we have discussed elsewhere [11], and weak uniform seed fields have been used in many previous studies of turbulent magnetic dynamo [60, 61, 66]. Thus, at fixed $\mathbf{r}$, the magnetic correlation function with this initial seed field is dominated at long times t by the leading dynamo eigenmode $\mathcal{E}$,

$$\langle B^i(\mathbf{r}, t) B^j(\mathbf{0}, t) \rangle \sim (\text{const.}) e^{\gamma t} \mathcal{E}^{ij}(\mathbf{r}), \quad t \to \infty$$

with γ the dynamo growth rate. In the opposite limit of large distances for fixed t it follows from (43),(45) that

$$\langle B^i(\mathbf{r}, t) B^j(\mathbf{0}, t) \rangle \sim \frac{1}{3} \delta^{ij}, \quad |\mathbf{r}| \to \infty$$

for our choice of initial seed field.

We implemented this scheme numerically by solving the SDE (29) backward in time for $N = 1024$ samples $\widetilde{\mathbf{a}}^n(\tau)$, $n = 1, 2, \ldots N$, all started from point $\mathbf{x}$ at time t_f with independent realizations of the noise. We took $t_f = 1.5$ and $t_0 = 0.5$, because the spatially-averaged energy dissipation $\varepsilon(\tau)$ is very constant for the interval of time $t_0 < \tau < t_f$ in the database, varying by $< 1\%$ from its space-time mean value $\bar{\varepsilon} = 0.0919$ over that interval. As in our study of Richardson diffusion, we solved (29) using the Euler-Maruyama scheme with $dt = 10^{-3}$ and solved the equation (46) for $\boldsymbol{\mathcal{J}}$ with the Euler method. Velocity-gradients are calculated by a 4th-order finite-difference scheme with 4th-order Lagrange interpolation

in space. We checked convergence in dt for several $\mathbf{x}$ values both by taking smaller dt and by comparison with the 1.5th-order method of Platen for (29) and a consistent scheme for the matrix $\mathcal{J}$. We then approximated

$$\langle B^2(\mathbf{x}, t_f) \rangle_\tau \doteq$$
$$\frac{2}{N(N-1)} \sum_{1 \leq n < m \leq N} \frac{1}{3} \text{tr} \left(\mathcal{J}(\widetilde{\mathbf{a}}^n, t_f, \tau) \mathcal{J}^\top(\widetilde{\mathbf{a}}^m, t_f, \tau) \right), \tag{48}$$

by a sum over the $N(N-1)/2 = 523,776$ number of pairs of samples. Note that Hoeffding's law of large numbers for U-statistics [67, 68] implies that this pair-average converges for $N \to \infty$ to the double-average in (47) over two independent realizations of the white-noise. We then furthermore averaged in space over $S = 1600$ points $\mathbf{x}_s$, $s = 1, 2, \ldots S$, with 25 points chosen randomly from each of $64 = 4^3$ subcubes of the whole domain. We obtain

$$\langle B^2(t) \rangle \doteq \frac{1}{S} \sum_{s=1}^{S} \langle B^2(\mathbf{x}_s, t_f) \rangle_\tau \tag{49}$$

as our final approximation to the magnetic energy. More space-averaging was required for the kinematic dynamo than for Richardson diffusion because of intermittency of the velocity-gradients involved in line-stretching [69].

2. Results

We now present our results for $Pr_m = 1$. We first demonstrate convergence of our algorithm in S and N. There are several ways to estimate the errors associated with the averaging over space and random samples. One approach is to consider the approximation to the Cauchy-Green matrix $\mathbf{F}$ obtained by omitting the $\frac{1}{3}$ factor and the trace in eq.(48). As we have discussed above, the exact Cauchy-Green matrix should be a positive-definite, symmetric matrix. Thus, if we form the symmetric and anti-symmetric parts

$$\mathbf{F}_S = \frac{1}{2}(\mathbf{F} + \mathbf{F}^\top), \quad \mathbf{F}_A = \frac{1}{2}(\mathbf{F} - \mathbf{F}^\top),$$

one measure of the relative error in our calculation is the ratio of matrix norms

$$\rho(t) = \frac{\|\langle \mathbf{F}_A(t_f, \tau) \rangle\|}{\|\langle \mathbf{F}_S(t_f, \tau) \rangle\|}.$$

Furthermore, if the small-scale turbulence is statistically isotropic (as is known for the database employed), then the space-average Cauchy-Green matrix should satisfy

$$\langle F_{ij} \rangle = \frac{1}{3} \text{tr} (\langle \mathbf{F} \rangle) \delta_{ij}.$$

In particular, each of the three eigenvalues $\phi_i(t)$, $i = 1, 2, 3$ of $\langle \mathbf{F}(t_f, \tau) \rangle$ should be equal to $\langle B^2(t) \rangle$.

In Fig. 5 (a) and (b) we plot our results for $\rho(t)$ and $\phi_i(t)$, $i = 1, 2, 3$, respectively. Note that time t
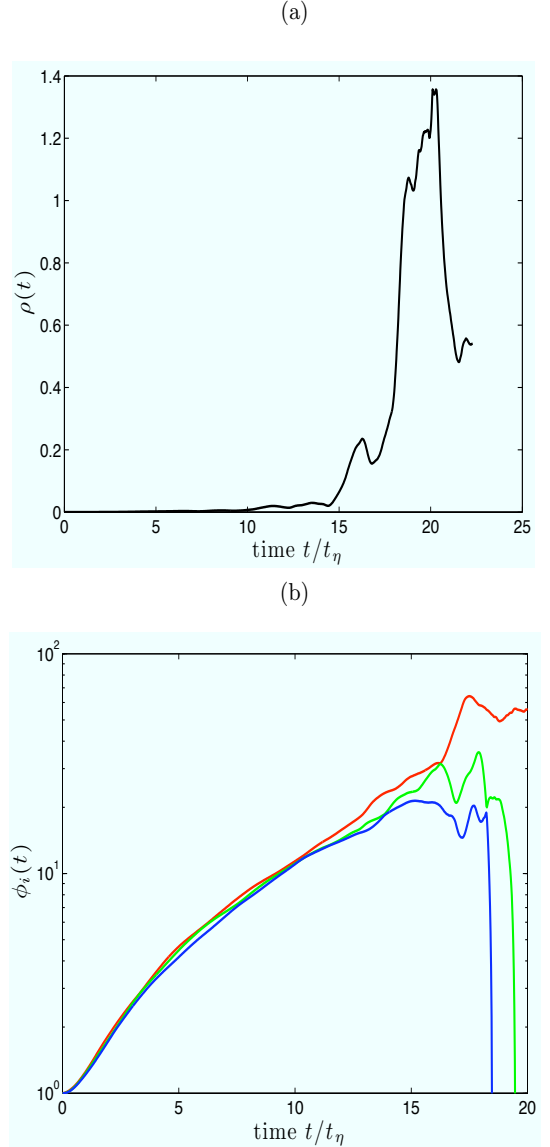

(a)

(b)

FIG. 5. (Color) Error estimation. (a) The ratio $\rho(t)$ of the norms of the anti-symmetric and symmetric parts of the approximate Cauchy-Green tensor. (b) The eigenvalues $\phi_i(t)$, $i = 1, 2, 3$ of the approximate Cauchy-Green tensor, with red for largest, green for middle, and blue for smallest.

in these plots and in all those following has been non-dimensionalized by the resistive time $t_\eta = \sqrt{\lambda/\bar{\varepsilon}} = 4.49 \times 10^{-2}$ (which is also the viscous time since $Pr_m = 1$). The results for $\rho(t)$ show that the relative error in our calculation is less than a few percent up until about 15 resistive times. This is confirmed by the plot of the three eigenvalues $\phi_i(t)$, $i = 1, 2, 3$, in panel (b), which are in quite close agreement until that time. The eigenvalues also remain all positive until after 18 resistive times, consistent with positivity of $\langle B^2(t) \rangle$. These results show, incidentally, that there was no need for us to take the initial magnetic

field $\mathbf{B}_0$ to be random and statistically isotropic. The same dynamo growth is observed for any deterministic uniform field pointing in any direction.

The error in our approximation for $\langle B^2(t) \rangle$ can also be estimated in the same way as was the error for the Richardson 2-particle dispersion in section II.C. Since the number of pairs in (48) is quite large, one can guess that the dominant error arises from the average over S space points in (49). A central limit theorem argument then suggests that the error is approximated by

$$\delta \langle B^2(t) \rangle \simeq \sqrt{\frac{\text{Var}\left\{\langle B^2(t_f) \rangle_\tau\right\}}{S}} \qquad (50)$$

with the spatial variance

$$\text{Var}\left\{\langle B^2(t_f) \rangle_\tau\right\} \doteq \frac{1}{S-1} \sum_{s=1}^{S} \left| \langle B^2(\mathbf{x}_s, t_f) \rangle_\tau - \langle B^2(t) \rangle \right|^2. \qquad (51)$$

This latter quantity has some independent physical interest, because it quantifies the spatial intermittency of the dynamo effect. In Fig. 6 we plot our approximation (49) for $\langle B^2(t) \rangle$ along with plus-or-minus the error estimate $\delta \langle B^2(t) \rangle$ above. These are consistent with the estimates in the previous Fig. 5.

The plot of magnetic energy from kinematic dynamo effect in Fig. 6 is our central result in this section. The expected exponential growth $\sim e^{\gamma t}$ of magnetic energy is clearly observed after about 6 resistive times. A linear fit over the range of times 6 to 16 is also plotted in Fig. 6, yielding an estimated growth rate of $\gamma t_\eta \doteq 0.158$. At earlier times the growth rate is significantly larger. For example, a linear fit over the range of 1 to 4 resistive times yields an estimate $\gamma t_\eta \doteq 0.344$. This is closer to the magnitude of the typical viscous strain rate eigenvalue $\sqrt{\langle S^2 \rangle / 3}$, which in units of the viscous/resistive rate $\sqrt{\bar{\varepsilon}/\nu}$ is equal to $1/\sqrt{6} \doteq 0.408$. The physical interpretation of these results is clear. According to the stochastic Lundquist formula (32), field lines that are carried into a point $\mathbf{x}$ along individual Lagrangian trajectories are stretched at the viscous strain rate. However, the resistive average over the ensemble of stochastic trajectories leads to cancellation and suppression of the growth rate. As time advances, the spatial region sampled by the wandering trajectories increases in size and the suppression effect increases. Indeed, the asymptotic exponential growth range begins precisely at the onset of turbulent Richardson diffusion of the trajectories. To demonstrate this, we consider the (backward) dispersion $\langle r^2(t) \rangle$ of the stochastic Lagrangian trajectories which determines the typical linear dimension $L(t) = \sqrt{\langle r^2(t) \rangle}$ of the region from which field-lines arrive. The local-in-time scaling exponent

$$\sigma(t) \equiv \frac{d \log(\langle r^2(t) \rangle)}{d \log(t)}. \qquad (52)$$

will equal 1 at early times and transition to 3 when Richardson diffusion sets in. The numerical results for
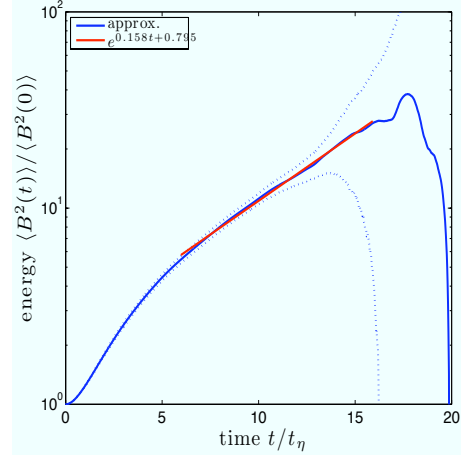

FIG. 6. (Color) Mean magnetic energy. Plotted in blue is the mean magnetic energy (solid line) calculated from (48),(49), along with plus and minus the error (dotted line) estimated from (50),(51). The straight line in red shows the least-square linear fit over the time interval $t=6$ to $t=16$.
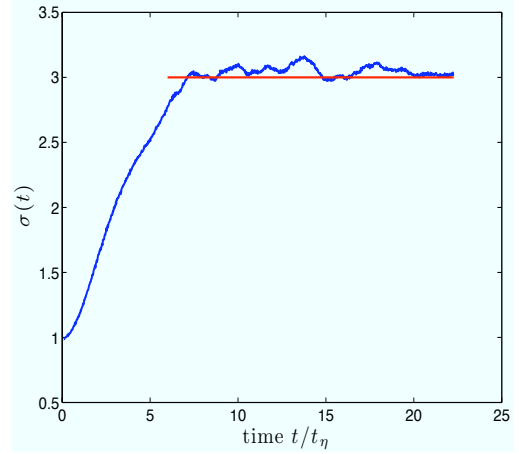

FIG. 7. (Color) Local slope of backward dispersion. Plotted in blue is the local slope of the backward dispersion $\langle r^2(t) \rangle$, as defined in (52). Plotted in red is the horizontal line-segment from $t=6$ to $t=25$ for the Richardson value $\sigma = 3$.

this quantity are plotted in Fig. 7, along with a horizontal line (red) at level $\sigma = 3$ beginning at $t = 6$. It is clear that the asymptotic exponential growth range of magnetic energy and the Richardson diffusion of trajectories start at the same time. The inertial-range properties of turbulent 2-particle diffusion are thus critical in determining the ultimate growth rate of the $Pr_m = 1$ turbulent kinematic dynamo.

Although initial field lines arrive to a point at time t from a large region of size $L(t)$, not all of these field lines contribute equally to the growth of magnetic energy. To quantify the contribution of line-vectors at initial separation r, we use the line-vector correlation function which was proposed as a "dynamo order-parameter" [10]:

$$\mathcal{R}_{k\ell}(\mathbf{r}, t) = F_{k\ell}^{ii}(\mathbf{r}, t_0 | \mathbf{0}, t),$$

where F is the homogeneous 2-particle Green's function from (44) [70]. $\mathcal{R}_{k\ell}(\mathbf{r}, t)$ represents the scalar correlation at time t between material line-vectors $\boldsymbol{\ell}(t)$, $\boldsymbol{\ell}'(t)$ which started as unit vectors $\hat{\mathbf{e}}_k$, $\hat{\mathbf{e}}_\ell$ at positions displaced by $\mathbf{r}$ at the initial time 0 and which arrive at the same final point. Setting $r = 0$ in eq.(43) gives, in general,

$$\langle B^2(t) \rangle = \int d^3 r \, \langle B_0^k(\boldsymbol{\rho}) B_0^\ell(\mathbf{0}) \rangle \mathcal{R}_{k\ell}(\boldsymbol{\rho}, t).$$

This formula separates the effect of the initial correlations of the magnetic field and the effect of the turbulent advection and stretching. For the case of isotropic and non-helical velocity statistics, we may decompose the tensor $\mathcal{R}$ into contributions from line-vectors initially longitudinal and transverse to the separation vector $\mathbf{r}$:

$$\mathcal{R}_{k\ell}(\mathbf{r}, t) = R_L(r, t) \hat{r}_k \hat{r}_\ell + R_N(r, t)(\delta_{k\ell} - \hat{r}_k \hat{r}_\ell),$$

where $\hat{\mathbf{r}}$ is the unit vector in the direction of $\mathbf{r}$. For our particular choice of uniform initial magnetic field,

$$\langle B^2(t) \rangle = \frac{1}{3} \int_0^\infty 4\pi r^2 dr \, [R_L(r, t) + 2R_N(r, t)]. \quad (53)$$

This line-correlation can be calculated numerically by the same procedure that we have used to obtain the magnetic energy itself in eqs.(48) and (49). For example, the longitudinal line-correlation can be approximated by

$$R_L(r, t) \doteq$$
$$\frac{1}{S} \sum_{s=1}^{S} \frac{2}{N(N-1)} \sum_{n<m} \hat{\mathbf{r}} \boldsymbol{\mathcal{J}}(\widetilde{\mathbf{a}}_s^n, t_f, \tau) \boldsymbol{\mathcal{J}}^\top(\widetilde{\mathbf{a}}_s^m, t_f, \tau) \hat{\mathbf{r}}^\top$$
$$\times \frac{\delta(|\widetilde{\mathbf{a}}_s^n(\tau) - \widetilde{\mathbf{a}}_s^m(\tau)| - r)}{4\pi r^2}, \quad (54)$$

taking $\hat{\mathbf{r}}$ as a row vector. The corresponding transverse correlation $R_N(r, t)$ is obtained by replacing $\hat{\mathbf{r}}$ in (54) with two orthogonal unit vectors $\hat{\mathbf{e}}_i$, $i = 1, 2$ which span the subspace orthogonal to $\hat{\mathbf{r}}$ and by then summing over these two contributions. In practice these continuous distributions must be sampled in discrete bins. We took 200 bins of size $\Delta r = \ell_\eta/2$, or one-half of the resistive length-scale. To capture the contributions from $r > 100\ell_\eta$ but to avoid large fluctuations in the results, we added three extra large bins of size $100, 200$, and $400 \, \ell_\eta$, centered at $150, 300$ and $600 \, \ell_\eta$, thus covering the whole range of r in the database.

We present in Fig. 8 our numerical results for $R_L(r, t)$ and $R_N(r, t)$ at a time $t = 11.12$ in resistive time-units.
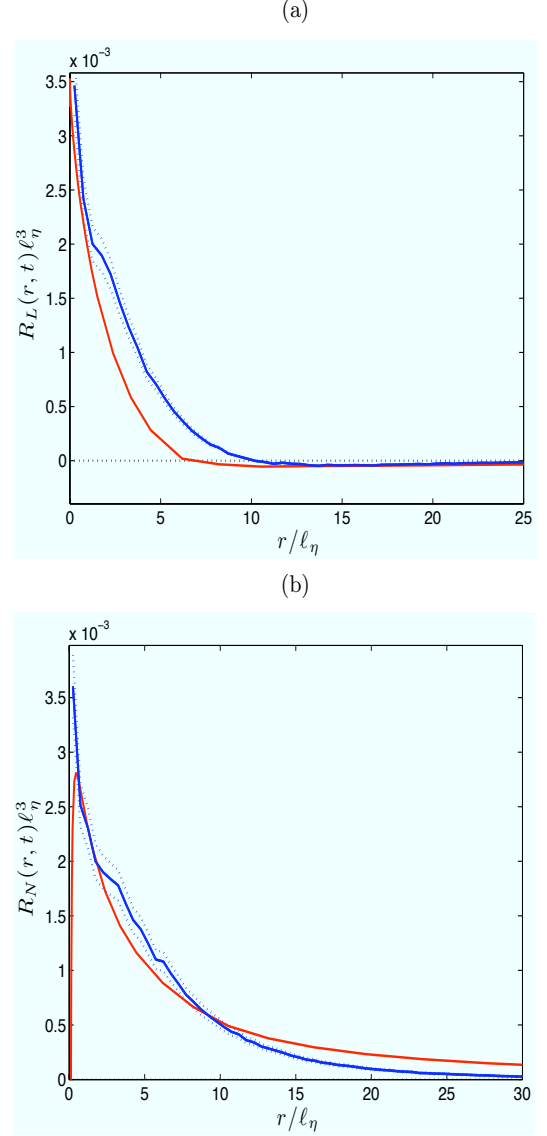

FIG. 8. (Color) Line-vector correlations: (a) longitudinal, (b) transverse. The line-vector correlations $R_L(r, t)$ and $R_N(r, t)$, respectively, as calculated numerically from formula (54) at time $t = 11.12$, are plotted in blue with solid lines and the correlations plus and minus their estimated errors with dotted lines. Also plotted with red lines are analytical results [11] for these correlations in the Kazantsev-Kraichnan model at $Pr_m = 0$, normalized as described in the text.

As should be clear from Figs. 6 and 7, this time lies well within the range both of exponential growth of energy and of Richardson diffusion of particle pairs. The most interesting feature of these correlations is their considerable diffuseness in r. This is shown even more clearly in Fig. 9, which plots the integrands $4\pi r^2 R_L(r, t)$ and $4\pi r^2 R_N(r, t)$ in eq.(53) for $\langle B^2(t) \rangle$. In order to get 50% of the magnetic energy one must integrate in that for-
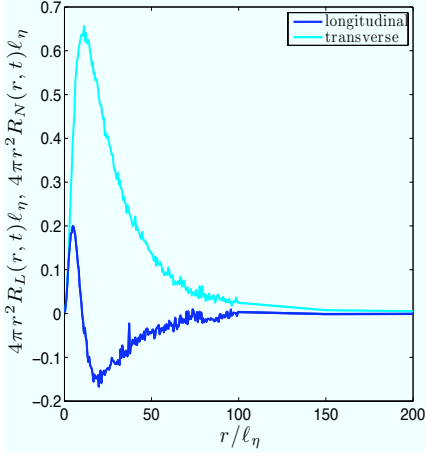
FIG. 9. (Color) Contributions to magnetic energy. Plotted in blue is the function $4\pi r^2 R_L(r,t)$ and in cyan the function $4\pi r^2 R_N(r,t)$, both at time $t = 11.12$. These represent the contributions to magnetic energy in (53) from pairs of line-vectors at initial separations r and initially parallel and perpendicular, respectively, to the separation vector **r**.

mula out to $r = 15.71\ell_\eta$. Likewise, to get 75% of the energy one must integrate out to $r = 39.15\ell_\eta$ and to get 90% one must integrate all the way out to $r = 66.59\ell_\eta$. Thus, line-vectors separated initially by many resistive lengths are brought together by turbulent advection to produce the dynamo growth. Another very interesting feature is the large *negative* contribution of the initially longitudinal line-vectors, seen in Fig. 8(a) and even more clearly in Fig. 9. A very similar negative contribution was found [11] for the Kazantsev-Kraichnan dynamo model at $Pr_m = 0$ and $Rm = \infty$. It was suggested there that negative values of $R_L(r,t)$ for sufficiently large r are due to an effect of bending and looping of field lines.

It is interesting to make a more detailed comparison of our numerical results for hydrodynamic turbulence at $Pr_m = 1$ and of the analytical results in the Kazantsev-Kraichnan (KK) dynamo model for $Pr_m = 0$. The comparison is not completely straightforward, so a few words of explanation are required. We consider the KK model with spatial Hölder exponent $h = 2/3$ in the velocity correlation (15). With this choice of h, Richardson's t^3-law holds for particle dispersion and it is generally the appropriate choice for comparisons with physical fluid turbulence. In this case, the coefficient D_1 in (15) has the same dimensions as $\varepsilon^{1/3}$, with ε the mean energy dissipation per unit mass. Our previous results for the KK model [10, 11] were obtained with lengths non-dimensionalized by $(\lambda/D_1)^{3/4}$ and times by $(\lambda/D_1^3)^{1/2}$. However, D_1 is not numerically equal to $\varepsilon^{1/3}$, but only dimensionally the same. In order to relate them quantitatively, we note that the KK particle diffusion equation (16) reduces in the

isotropic sector to Richardson's original equation (2) with coefficient of eddy-diffusivity $K_0 = 2D_1$. In that case, one recovers the t^3-law (6) with a Richardson-Obukhov constant g_0 if one makes the definition for the KK model

$$\varepsilon \equiv 143\frac{64}{81g_0}D_1^3. \tag{55}$$

We thus obtain $\ell_\eta \equiv (\lambda^3/\varepsilon)^{1/4} = \beta(\lambda/D_1)^{3/4}$ with $\beta = \frac{3}{2\sqrt{2}}\left(\frac{g_0}{143}\right)^{1/4}$. For the backward 2-particle diffusion in our kinematic dynamo study we have found that $g_0 \doteq 1.57$ (somewhat larger than the value 1.35 reported in section II.C for an independent experiment over a different time range) and thus $\beta \doteq 0.343$. For comparison with the present results, therefore, the results of Eyink [11], Fig. 10 must have x-axis scaled by $1/\beta$ and y-axis scaled by β^3. Furthermore, the quantities $\widetilde{G}_L(r)$, $\widetilde{G}_N(r)$ previously calculated [11] are dynamo growth eigenmodes which dominate the behavior of $R_L(r,t)$, $R_N(r,t)$ at long times. Since there is an arbitrariness in the normalization of the eigenmodes, we have additional freedom in the vertical scale. This is fixed by imposing on the KK eigenmodes the normalization condition (53) at $t = 11.12$ resistive time units.

We have plotted the results for the line-correlations from the KK model in Fig. 8 (red lines), together with our numerical results for hydrodynamic turbulence (blue lines). Clearly, the two sets of results are qualitatively very similar. In both cases, the transverse correlation $R_N(r,t)$ is everywhere positive, sharply peaked at small r, but with a slow decay at large r. The longitudinal correlations $R_L(r,t)$ of the two sets share all these same features except for their sign, with both exhibiting a long negative tail at large r. The major difference between the results for hydrodynamic turbulence at $Pr_m = 1$ and the KK model at $Pr_m = 0$ is the distinctly slower rate of decay of correlations at large r for the latter.

The precise decay rate at large r is known for the line-correlations in the KK model. It was shown [11] that, up to power-law prefactors, these exhibit a very slow stretched-exponential decay

$$\widetilde{G}_L(r), \widetilde{G}_N(r) \sim \exp\left(-\frac{3\sqrt{2\gamma}}{2D_1}r^{1/3}\right), \quad r \gg \ell_\eta, \tag{56}$$

where γ is the dynamo growth rate. A remarkable feature of this asymptotic formula is that it depends upon resistivity η (or magnetic diffusivity $\lambda = \eta c/4\pi$) only through the growth rate γ. To check for a similar decay in hydrodynamic turbulence we present in Fig. 10 (a),(b) a log-linear plot of the line-correlations $|R_L(r,t)|$, $R_N(r,t)$ versus $r^{1/3}$, both for our numerical calculation with the hydro turbulence database (blue) and for the KK model (red). The straight lines in these plots verify the stretched exponential decay with power $r^{1/3}$. In fact, the decay law (56) which was derived in the KK model for $Pr_m = 0$ holds very well in hydrodynamic turbulence at $Pr_m = 1$, including the coefficient in the
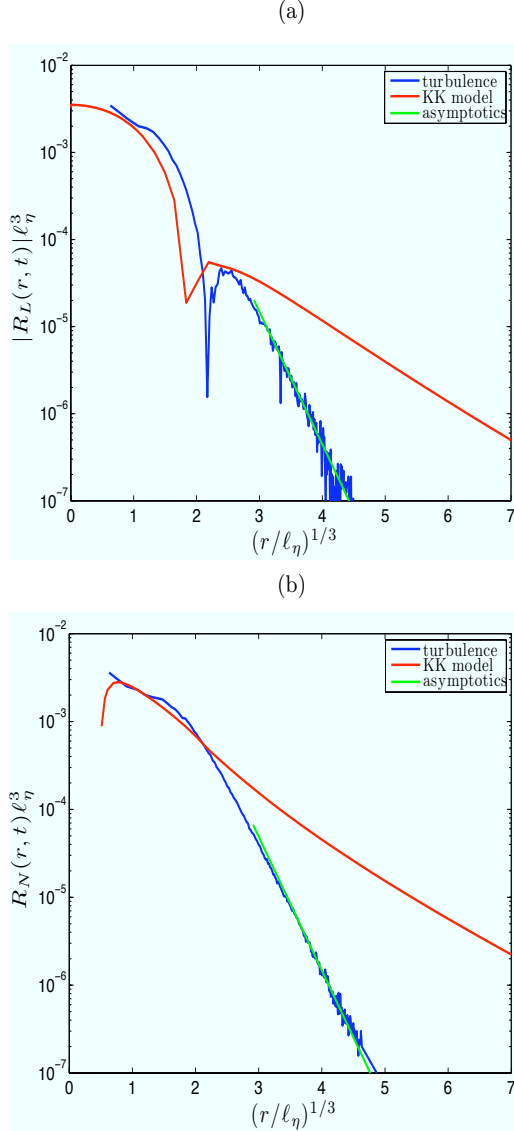
(a)

(b)

FIG. 10. (Color) Line-correlations for large separations: (a) longitudinal, (b) transverse. Plotted in blue are the numerical results from (54) at time $t = 11.12$ and in red the analytical results [11] from the Kazantsev-Kraichnan model at $Pr_m = 0$. Straight lines in the log-linear plot versus $r^{1/3}$ correspond to the large-r asymptotics (56). Shown in green is the prediction of that formula with the growth rate $\gamma = 0.158$ determined in Fig. 6.

stretched exponential. If we use the relation (55) to replace D_1 with ε and then substitute the dynamo growth rate $\gamma t_\eta \doteq 0.158$, we predict from (56) a line in a log-linear plot with slope -3.507 (in resistive units). A line with this slope is plotted (in green) in Fig. 10 (a),(b) and can be seen to match our numerical results quite well. The reason for the slower decay of the stretched exponential in the KK model at $Pr_m = 0$ is thus entirely

attributable to a smaller dynamo growth rate than what we find in hydro turbulence for $Pr_m = 1$. In particular, using the result [11, 71] that $\gamma(\lambda/D_1^3)^{1/2} \doteq 0.193$ for KK at $Pr_m = 0$ and using again the relation (55), we get that $\gamma t_\eta \doteq 0.0217$. This is almost an order of magnitude smaller than the result $\gamma t_\eta \doteq 0.158$ that we found for hydro turbulence at $Pr_m = 1$ and motivates some further discussion below.

3. Discussion

Let us make a quantitative comparison of our growth rate with those found in other studies [17, 18, 60, 61, 71] of small-scale dynamo in incompressible, non-helical turbulence at $Pr_m = 1$. We present both the Reynolds numbers and the dynamo growth rates found in these studies. We give the "box-size" Reynolds number $Re = u'/\nu k_0$, where $u' = u_{rms}/\sqrt{3}$ is the rms value of a single velocity component and k_0 is the smallest wavenumber in the simulation study. This is not as dynamically significant a Reynolds number as is $Re_f = u_{rms}/\nu k_f$, based on the forcing wavenumber k_f, but it is the easiest to calculate from the published data. We give the growth rate in the dimensionless form γt_ν where, as above, $t_\nu = (\nu/\varepsilon)^{1/2}$ is the viscous time (and also the resistive time for $Pr_m = 1$). The data from the paper of Schekochihin et al. (2004) [18] is taken from their Table 2 (where $1/t_\nu = \sqrt{15}\Gamma_{rms}$ there). The data of Haugen et al. (2004) [17] is taken from their Fig.3, which plots their results for $\alpha \equiv (\gamma/2)/(u_{rms}k_f)$ versus Re_f. Note, however, that

$$\gamma t_\nu = 2\alpha\sqrt{\frac{3}{5}\frac{Re_T}{Re_f}},$$

where $Re_T = u'\ell_T/\nu$ is the Taylor-scale Reynolds number defined there [17], with $\ell_T = \sqrt{5}u_{rms}/\omega_{rms}$. We can also infer from their Table II [17] that $Re_T = \sqrt{60Re_f}$ so that, putting all these relations together,

$$\gamma t_\nu = \frac{12\alpha}{\sqrt{Re_f}}.$$

Finally, $Re = \frac{\sqrt{3}}{2}Re_f$ since their forcing wavenumber [17] is $k_f = 1.5$ and $u' = u_{rms}/\sqrt{3}$. The paper of Vincenzi (2002) [71] presents a numerical study of the KK model. Fig. 6 in that work plots the results for $\gamma(\lambda/D_1^3)^{1/2}$ at $Re = \infty$ and a broad range of Prandtl numbers. Note that the "viscosity" for the KK model is defined [71] by $\nu_* = D_1\ell_\nu^{4/3}$ where ℓ_ν is the short-distance cut-off length of the inertial scaling range and the corresponding "Prandtl number" is defined by $Pr_{m*} = \nu_*/\lambda$. It is not obvious how to best compare this "Prandtl number" with that for viscous hydrodynamic turbulence. In any case, the result for $Pr_{m*} = 1$ is $\gamma(\lambda/D_1^3)^{1/2} \doteq 0.350$, which we transform to $\gamma t_\nu \doteq 0.0383$ as described earlier. Finally, the papers of Cho et al. [60, 61] present results

for a large number of runs with both normal and hyper-viscosity. The authors have kindly provided data from their highest Reynolds-number normal-viscosity simulation, denoted RUN $512P - B_0 10^{-3}$ (for 512^3 resolution with physical viscosity and initial uniform seed field of strength 10^{-3}.) This data is reported below (J. Cho, private communication). In one important respect this simulation is quite distinct from the others reported here, because the initial velocity field is not a fully developed turbulent field but is instead supported in the very low-wavenumber interval $2 \leq k \leq 4$. Turbulence quickly develops with the volume-averaged kinetic energy dissipation $\varepsilon(t)$ increasing by a factor of 42 over their time interval of kinematic dynamo. Although this dynamo simulation is not in a statistically steady turbulent regime, it does give some useful perspective and we thus include it here. All of these data are gathered into Table I below.

TABLE I. Reynolds numbers and dynamo growth rates from several numerical studies with $Pr_m = 1$. Shown are the box-size Reynolds number $Re = u'/\nu k_0$, where k_0 is the minimum wavenumber, and the growth rate γ non-dimensionalized by the viscous time $t_\nu = (\nu/\varepsilon)^{1/2}$.

Reference	Re	γt_ν
Schekochihin et al. (2004)	110	0.0138
	210	0.0265
	450	0.0329
Haugen et al. (2004)	131	0.0338
	260	0.0379
	606	0.0385
Vincenzi (2002) [KK model]	∞	0.0383
Cho et al. (2009)	294	0.550
present study	6380	0.158

It is widely expected that γt_ν approaches a universal value as $Re \to \infty$, but the data presented seem not to confirm this. The study of Haugen et al. [17] indeed reported seeing such a limiting behavior, as can be observed from their data in Table I. Their results for the growth rate are also consistent with those of Schekochihin et al. [18] and remarkably close to those of Vincenzi [71] for the KK model at $Re = \infty$. The latter must be regarded as a coincidence, however, due to the ambiguity in the definition of the Prandtl number for that model. For example, a better definition might be $Pr_m \equiv \epsilon^{1/3} \ell_\nu^{4/3}/\lambda$, which, using (55), gives $Pr_m \doteq 4.16 Pr_{m*}$. Thus, $Pr_m = 1$ corresponds to $Pr_{m*} \doteq 0.24$. Whatever the "best" definition of the Prandtl number for the KK model might be, the value of γt_ν for $Pr_m = 1$ will be somewhat smaller than that reported above for $Pr_{m*} = 1$, because the latter is near the maximum of $\gamma(\lambda/D_1^3)^{1/2}$ (Vincenzi [71], Fig. 6). Our own result for γt_ν is about 4 times larger than the value of Haugen et al. for their highest Reynolds number simulation. The dimensionless growth rate increases with Re and our Reynolds number is about 6 times larger than theirs, so this might account for some of the discrepancy.

On the other hand, our resolution of the viscous range is also relatively poor and this may degrade the numerical accuracy of our result for the growth rate. To further complicate the picture, the value of γt_ν found by Cho et al. is about 3.5 times larger than ours. Note that the result reported in Table I for Cho's data used the value $\bar{\varepsilon}$ from a time-average of $\varepsilon(t)$ over the kinematic interval of exponential growth in order to define t_ν. If we instead used the value $\varepsilon(t_*)$ at the end of the kinematic interval to define t_ν, then we would obtain a somewhat smaller value $\gamma t_\nu \doteq 0.312$ for Cho et al. but still twice ours.

The results in the Table I appear contradictory on the face of it, but we believe there is a simple resolution. The key is the time range over which the exponential growth is observed. Our growth rate was calculated for the time interval 6–$16 t_\nu$ with the latter time only about $1/3$ T_u, where $T_u = L_u/u'$ is the large-scale eddy-turnover time. Haugen et al. do not publish growth curves in their paper, but Schekochihin et al. present in their Fig. 21[18] a log-linear plot of the magnetic energy for their kinematic runs, with fitting ranges for exponential growth indicated. The cited growth rate for their 450 Reynolds-number simulation (Run A) was obtained over a time-interval of 66.6–$505.9 t_\nu$. This corresponds in their simulation to about 5.86–$44.5 T_u$. (Here we have used the well-known result that $T_u \doteq 0.4(u')^2/\varepsilon$ and the data in their Table 1 [18] to estimate $T_u \doteq 0.267$ for Run A.) At earlier times in their simulation, the growth of magnetic energy is much faster. For example, if we use the data in their Fig. 21 for times $< 5.86 T_u$ to estimate the growth rate, we obtain a value $\gamma t_\nu = 0.0691$, about half of ours.

We therefore conjecture that there are two distinct kinematic regimes with exponential growth of magnetic energy at different rates, one for times $t \ll T_u$ and another for times $t \gg T_u$. This makes perfect sense from the Lagrangian point of view developed in this paper. For times $t \ll T_u$, the (backward) particle dispersion $\langle r^2(t) \rangle$ is growing as $\sim \varepsilon t^3$ (see Fig. 7). This means that the magnetic field strengths are obtained by averaging initial field vectors arriving from inertial-range separations growing as a power-law. However, for times $t \gg T_u$, the mean-square separation $\langle r^2(t) \rangle$ saturates to a value of order $\sim L_B^2$, where L_B is the size of the periodic box. In this time regime, therefore, magnetic field strengths are obtained by averaging seed field vectors arriving to each point from the entire flow domain. Furthermore, each initial line-vector that arrives to a point will have moved a distance of order $u_{rms} t \gg L_B$ and has thus generally crossed the entire periodic domain a large number of times. It stands to reason that the growth rate would be reduced in this strongly mixed regime. Which of the two kinematic regimes is most relevant in practice depends upon the strength of the seed magnetic field B_0. It is observed [17, 18, 60] that the kinematic interval of exponential growth ends once the magnetic field energy $\langle B^2(t) \rangle$ grows to equipartition with the viscous-range kinetic energy $u_\nu^2 = (\varepsilon \nu)^{1/2}$. If $\ln(u_\nu/B_0) \ll \gamma T_u = O((Re)^{1/2})$, then this occurs at times much less than T_u, the regime

that we have studied. This will be the typical situation at high Reynolds numbers. On the other hand, if the seed field is exponentially small for large Re (i.e. $B_0 < u_\nu e^{-O(Re^{1/2})}$) or if the Reynolds number is not so large, then viscous equipartition will only occur for times $\gg T_u$. This is the regime studied in Shekochihin et al. [18]and Haugen et al. [17]. In support of this conclusion, we note that the RUN $512P - B_0 10^{-3}$ of Cho et al., with a not too small seed field, reached saturation with viscous kinetic energy at a time around $12t_\nu$ or $1.2T_u$. The growth rate cited in Table I was obtained from a fit over the range 1.72–11.7t_ν or 0.173–1.18T_u, comparable to the time range that we study, and with a similarly large growth rate.

Clearly more study of this matter would be desirable. Unfortunately, the turbulence database that we employ only stores the velocity field for about one T_u, or $44.8t_\nu$, so we cannot study times $\gg T_u$. We do believe, however, that our results have attained the asymptotic regime $t_\nu \ll t \ll T_u$. In support of this claim, we note that we are observing already at time $11.12t_\nu$ the expected inertial-range behaviors, such as Richardson diffusion and the stretched-exponential correlation decay in eq.(56) (which was derived in the KK model for $L_u = \infty$).

The most important general conclusion from our results presented above is that the inertial-range phenomenon of Richardson diffusion plays a critical role in the small-scale fluctuation dynamo of hydrodynamic turbulence at $Pr_m = 1$. Because field lines are only "frozen-in" stochastically, an infinite number of lines enters each point from a very large region of size $L(t) \sim (\varepsilon t^3)^{1/2}$ at time t. This mixing of field lines from far away opposes the growth by stretching of the individual lines and suppresses the dynamo growth rate. Because of nearly complete cancellation, the lines arriving from separations of order $\sim L(t)$ contribute a vanishingly small amount to the magnetic energy. Nevertheless, the asymptotic formula (56) shows that field-lines separated at inertial-range distances $r \gg \ell_\eta$ give a non-negligible contribution. That formula implies also—very remarkably— that the dynamo growth rate can be inferred directly from the stretched-exponential decay of the magnetic line-vector correlations in the inertial range.

A second important conclusion is that there are very fundamental similarities between the mechanisms of the small-scale fluctuation dynamo for Prandtl numbers $Pr_m = 1$ and $Pr_m = 0$ in high Reynolds-number turbulence. The physics that we have discussed above for hydrodynamic turbulence at $Pr_m = 1$ and large Rm agrees very closely with what was established [10, 11] for the Kazantsev-Kraichnan model at $Pr_m = 0$ and $Rm = \infty$. Richardson diffusion and stochasticity of flux-freezing play a critical role in both. This contradicts a view that inertial-range time-scales are too long to affect the operation of the dynamo, which proceeds at a faster viscous rate [18]. Because the exponential dynamo growth is a *long-time* phenomenon, there is sufficient time for advection by inertial-range eddies to affect and mod-

ify its rate. Indeed, we have seen in the present study at $Pr_m = 1$ that the inertial-range phenomenon of Richardson diffusion starts at times $t \gtrsim 6t_\nu$ and not at times orders of magnitude greater than the viscous time.

In our view, the $Pr_m = 1$ small-scale dynamo—and, more generally, the finite Pr_m dynamo— is a transitional case which shares some of the attributes of both of the extreme limits $Pr_m = 0$ and $Pr_m = \infty$. A corollary of this view is that there should be an important influence of the inertial range even for small-scale dynamos with $Pr_m \gg 1$, if also $Re \gg 1$. This is the situation for many low-density, high-temperature astrophysical plasmas with large magnetic Prandtl numbers but with, also, a substantial inertial range. As we have discussed in section II.B, the exponential separation of particles typical of the large-Pr_m "Batchelor regime" is an intermediate asymptotics for a range of times $t_\nu \ll t \ll \ln(Pr_m)t_\nu$ in high Reynolds-number turbulence. After a time $t \gtrsim t_\nu \ln(Pr_m)$, magnetic line-elements in such a turbulent flow will begin to experience Richardson diffusion and a concomitant decrease of the dynamo growth rate. Because the dependence upon Pr_m is logarithmic, the time to enter this inertial-range influenced regime is only a relatively small multiple of t_ν even at very large Pr_m. (For example, with a value $Pr_m = 10^{14}$ typical of the warm interstellar medium, $\ln(Pr_m) \doteq 32$.) If the initial magnetic seed field is weak enough, then its backreaction on the turbulence up to that time may be neglected and the turbulent kinematic dynamo process essentially as we have discussed in this section of our paper will proceed, even at very large Prandtl numbers.

V. NONLINEAR MHD TURBULENCE, DYNAMO AND RECONNECTION

Although we have focused in our discussion of dynamo effect on the kinematic stage, almost all of the results of this paper extend—with appropriate modifications— to fully nonlinear MHD turbulence with backreaction on the flow from the Lorentz force. A full treatment is not possible here, but we shall try to stress what is general in our previous presentation, sketch any necessary modifications, discuss relevant references, and point out some important directions for further work.

The phenomenon of 2-particle Richardson diffusion and "spontaneous stochasticity" will doubtless exist in MHD turbulence. Their cause is the roughness of the advecting velocity field and all theories, simulations and observations of MHD turbulence (whatever their other differences) agree that both the velocity and magnetic fields are indeed rough in the inertial-range of such flows. The quantitative growth law of particle dispersion will depend upon the precise characteristics of MHD turbulence, such as the spectral slopes, degree of anisotropy, etc. These depend upon the ultimate theory of MHD turbulence, which is an open problem. We base our discussion below on the Goldreich-Sridhar (GS) theory of

strong MHD turbulence [72, 73], but alternative theories would lead to similar results.

For simplicity, we assume incompressible and sub- or trans-Alfvénic MHD turbulence, with rms velocity fluctuations $u' \le v_A$, where $v_A = B_0/\sqrt{4\pi\rho}$ is the Alfvén velocity based on the external magnetic field strength B_0. We also assume that large-scale anisotropy is such that "critical balance" holds throughout the inertial range and the turbulence is strong. Finally, we assume that mean cross-helicity is zero and there is an equal flux of upward and downward propagating Alfvén waves. Under these conditions, the GS theory predicts that velocity increments for separations ℓ scale as

$$\delta u(\ell) \sim (\varepsilon\ell_\perp)^{1/3} \sim (\varepsilon\ell_\parallel/v_A)^{1/2},$$

where ε is energy dissipation per mass and $\ell_\perp, \ell_\parallel$ are the separations perpendicular and parallel to the magnetic field, respectively. We shall also assume that perpendicular (shear-Alfvén) and parallel (pseudo-Alfvén) components of the velocity increments scale in the same way, or $\delta u_\perp(\ell) \sim \delta u_\parallel(\ell)$. In that case, we can give a simple theory of particle-pair dispersion like that presented for hydro turbulence in section II.A. If we let $r_\perp(t)$ and $r_\parallel(t)$ be the particle separations perpendicular and parallel to the field, respectively, then

$$\frac{d}{dt}r_\perp \sim \delta u_\perp(r) \sim (\varepsilon r_\perp)^{1/3}$$

(assuming that $r_\parallel \equiv 0$) implies that

$$r_\perp^2(t) \sim \varepsilon t^3, \tag{57}$$

and in the same manner

$$\frac{d}{dt}r_\parallel \sim \delta u_\parallel(r) \sim (\varepsilon r_\parallel/v_A)^{1/2}$$

(assuming that $r_\perp \equiv 0$) implies that

$$r_\parallel^2(t) \sim (\varepsilon/v_A)^2 t^4. \tag{58}$$

The above scaling laws will hold for intermediate times where $t \gg (r_\perp^2(0)/\varepsilon)^{1/3}$, $(v_A r_\parallel(0)/\varepsilon)^{1/2}$ but $t \ll T_u = L_u/u'$, the large-eddy turnover time. The most important feature observed in both cases is that initial separations are "forgotten", the physical basis of the phenomenon of spontaneous stochasticity. A full theory of 2-particle dispersion in MHD turbulence will obviously be quite intricate and will depend upon the regime of turbulence considered and the phenomenological assumptions employed. Within theories of weak MHD turbulence [74], it should be possible to give an analytical treatment using well-established methods [75]. However, whatever final form the theory of MHD turbulence may take, spontaneous stochasticity seems to be a likely consequence.

There have been a few numerical studies of 2-particle dispersion in MHD turbulence, both with [76] and without [77, 78] external magnetic field. In the presence of an external magnetic field, Busse and Müller find that $r_\perp(t)$ grows faster than $r_\parallel(t)$ (see their Fig. 4 [76]), in qualitative agreement with our formulas (57) and (58) [79]. The situation is not entirely clear, however. Following Cho and Vishniac [66], it is generally believed that similar alignments and anisotropies will hold at small scales in MHD turbulence without an external magnetic field, just as for the external field case, if the alignments are taken with respect to a local magnetic field. Paradoxically, however, Busse et al. find in MHD turbulence without external field that $r_\perp(t) \ll r_\parallel(t)$ when these quantities are defined with respect to the local field. The total displacement vector $\mathbf{r}(t)$ thus becomes preferentially aligned with the local magnetic field. It is not obvious how to explain this observation, but it possibly has something to do with the dynamical alignment of velocity and magnetic-field increments at small scales [80, 81]. Clearly, more study of these issues is required.

Our results in section III.A on stochastic flux freezing in resistive magnetohydrodynamics were derived in a fully nonlinear setting. No kinematic assumption was made there. It has elsewhere been shown [45] that all effects of the Lorentz force on fluid motion are described by a second stochastic conservation law which generalizes the Kelvin circulation theorem, at least for incompressible fluids with $Pr_m = 1$. This result extends to resistive MHD the "generalized Kelvin theorem" derived for ideal MHD [82, 83]. As we shall show in a future paper, this additional stochastic Kelvin theorem also holds in compressible plasma fluids with $Pr_m = 1$ if they are barotropic (pressure depending only on density and not on temperature) and in non-isothermal fluids if the thermal Prandtl number is also unity. The existence of two stochastically "frozen-in" fields provides strong constraints which deserve to be further explored. We remark finally, and most importantly, that our discussion in section III.B on the high-Reynolds limit of plasma turbulence made no kinematic assumption. The prediction that stochastic flux-conservation holds in that limit depends only upon the phenomenon of spontaneous stochasticity, which we have argued should inevitably occur in high Reynolds-number plasma turbulence.

Perhaps the most important implications of the present work are for the problem of turbulent magnetic reconnection. Our results and arguments show compellingly, we believe, that the constraint of flux-freezing in a turbulent plasma at high-conductivity must be quite different than is generally understood. The naive estimate of flux-line slippage due to resistivity, $\langle r^2(t) \rangle \sim \lambda t$, is incorrect, by many orders of magnitude. The correct estimate will depend upon the ultimate theory of MHD turbulence, but it must have the general form of (57) and (58) above. The quantity $\sqrt{\langle r_\perp^2(t) \rangle}$ can be interpreted as the lateral distance that magnetic field-lines diffuse through a turbulent plasma in time t, and (57) should be particularly useful in estimating reconnection rates for astrophysical phenomena. Note that both (57) and (58) are completely independent of the resistivity (and of any other microscopic plasma mechanism of line-slippage). These results

give support, therefore, to all theories and observations of fast magnetic reconnection in MHD turbulence. In fact, our results show that fast reconnection is necessary for (implied by) all standard theories of MHD turbulence.

There are particularly close connections with the Lazarian-Vishniac theory [84] based on stochastic wandering of field-lines. We have stressed that Lagrangian particle trajectories become intrinsically stochastic in a rough velocity field, due to the phenomenon of Richardson 2-particle dispersion. The "stochastic wandering" invoked by Lazarian-Vishniac is an analogue of Richardson diffusion for the field lines themselves in a rough magnetic field. Because of this effect, there is not just one field-line passing through each point in the limit of zero resistivity, but instead an infinite ensemble of random field-lines. The connection between our ideas and those of Lazarian-Vishniac [84] deserve to be further examined.

VI. FINAL DISCUSSION

Two ideas are commonplace in the literature on plasma magnetohydrodynamics. One is that flux-freezing must hold approximately for $Rm \gg 1$, an assumption widely employed in treatments of magnetic dynamo effect. Another idea frequently advanced in discussion of magnetic reconnection is that the flux-freezing constraint is broken by rapid diffusion of field lines across thin current sheets. There has long been a tension between these two ideas, never fully reconciled. Both ideas are sometimes invoked in the same setting. For example, it is recognized that while stretching of "nearly" frozen-in lines drives magnetic dynamo action, nevertheless fast magnetic reconnection is necessary to relieve tangled field-line structure [84–86]. We have argued that *both* ideas are correct, if suitably understood. Magnetic flux through individual material loops, advected by the plasma in the usual sense, will *not* be conserved for $Rm \rightarrow \infty$, because of the development of singular current sheets and vortex sheets. However, magnetic flux in high-Reynolds-number MHD turbulence will nevertheless be conserved on average for a random ensemble of loops, in a novel statistical sense associated to the spontaneous stochasticity of Lagrangian flows.

Spontaneous stochasticity is a fluid-dynamical phenomenon due to the explosive separation of particles produced by turbulent Richardson diffusion. Because of this effect, fluid particles that start infinitesimally close together will separate to a finite distance in a fixed amount of time, independent of the Reynolds number. In the limit $Re \rightarrow \infty$ there is an infinite ensemble of Lagrangian trajectories for each initial particle position. There is already good evidence for this effect from turbulence simulations and laboratory experiments, much of which is reviewed in Section II.C together with own simulation results. We expect confirmation from future studies at higher Reynolds numbers. The Göttingen Turbulence Tunnel now in operation should reach Taylor-scale

Reynolds numbers $Re_T \sim 10^4$ and turbulent Richardson diffusion shall be one of the main subjects of investigation (E. Bodenschatz, private communication). Richardson diffusion and spontaneous stochasticity should also occur in high-Reynolds number MHD turbulence and can be studied by both simulation and experiment. Recent laboratory studies of magnetic dynamo and turbulent induction with low Prandtl-number liquid metals have Reynolds numbers high enough and inertial-ranges sufficiently extensive to support the phenomena. Although extremely challenging, it would be quite informative to develop particle-tracking techniques for such flows which could investigate Lagrangian mechanisms.

In an earlier work [87] we have considered Alfvén's theorem for turbulent plasma flows from a complementary perspective. The approach used there was a spatial coarse-graining of the MHD equations over a continuous range of scales ℓ, similar in spirit to a renormalization group analysis. The effective induction equation at length-scale ℓ contains a "turbulent electromotive force (EMF)" $\boldsymbol{\varepsilon}_\ell$ induced by subscale plasma motions. As long as energy remains finite for high kinetic and magnetic Reynolds numbers, the turbulent EMF can be shown to be much larger at inertial-range length-scales ℓ than viscous and resistive terms, or than other possible microscopic dissipation terms. In that case, the effective flux-conservation equation at inertial-range length-scales ℓ takes the form

$$\frac{d}{dt} \oint_{\overline{\mathbf{x}}_\ell(C,t)} \overline{\mathbf{A}}_\ell(\mathbf{x},t) \cdot d\mathbf{x} = \oint_{\overline{\mathbf{x}}_\ell(C,t)} \boldsymbol{\varepsilon}_\ell(\mathbf{x},t) \cdot d\mathbf{x}, \qquad (59)$$

where $\overline{\mathbf{A}}_\ell$ is the coarse-grained magnetic vector-potential and $\overline{\mathbf{x}}_\ell(\mathbf{a},t)$ is the Lagrangian flow map generated by the coarse-grained velocity field $\overline{\mathbf{u}}_\ell$. For a smooth, laminar solution of the ideal MHD equations, $\boldsymbol{\varepsilon}_\ell \rightarrow \mathbf{0}$ everywhere in space as $\ell \rightarrow 0$ and flux-conservation in the standard sense is recovered. However, it was shown [87] that the righthand side of (59) need not vanish for singular velocity and magnetic fields, for example, those with coincident "current sheets" and "vortex sheets" (more precisely, tangential discontinuities) or those for which advected loops become fractal. In such cases, Alfvén's theorem in its conventional sense can break down at infinite magnetic Reynolds number and magnetic flux $\overline{\Phi}_\ell(C,t) = \oint_{\overline{\mathbf{x}}_\ell(C,t)} \overline{\mathbf{A}}_\ell(\mathbf{x},t) \cdot d\mathbf{x}$ need no longer be conserved for individual loops C as $\ell \rightarrow 0$. Here we extend that conclusion by arguing that flux-conservation will hold *on average* for a suitable random ensemble of loops. Similarly as in section III.B, we may consider the set of loops $\overline{\mathbf{a}}_\ell(C + \epsilon\widetilde{C}, t)$ at time t_0 obtained by adding random perturbations of size ϵ to C and then advecting backward in time with $\overline{\mathbf{a}}_\ell(\cdot, t) = \overline{\mathbf{x}}_\ell^{-1}(\cdot, t)$. We expect that this ensemble of loops in the limits first of vanishing magnetic diffusivity and viscosity $\lambda, \nu \rightarrow 0$, then $\ell \rightarrow 0$ and finally $\epsilon \rightarrow 0$ will exactly coincide (at least for incompressible flow) with the ensemble $\widetilde{\mathbf{a}}^\lambda(C,t)$ for $\lambda, \nu \rightarrow 0$ considered in section III.A. If so, then flux-conservation will hold in an average sense similar to (35). The advantage of the

present argument is that it makes no explicit reference to Spitzer resistivity or to any other microscopic plasma mechanism. Stochastic flux-freezing is fundamentally a phenomenon of the nonlinear MHD dynamics.

Stochastic flux-conservation is expected to be a property of singular solutions of the ideal MHD equations that describe turbulent plasmas asymptotically at high kinetic and magnetic Reynolds numbers. The existence of such singular solutions is an old conjecture of Lars Onsager [88, 89]. Such solutions must be quite different from smooth laminar solutions of the ideal MHD equations that are familiar from current analysis, however, and must possess many "strange" properties. We are still learning how to deal with such solutions. We have recently shown how to derive the stochastic Kelvin theorem for the incompressible Navier-Stokes equation using a stochastic least-action principle [90]. It is expected that there will be a similar stochastic least-action principle for Onsager's singular Euler and ideal MHD solutions. This is a fundamental motivation to expect stochastic flux-conservation at infinite Reynolds numbers.

There must be many important applications of stochastic flux-freezing in plasma physics, astrophysics and geodynamo studies. We have here presented one concrete application to the finite-Pr_m, kinematic, fluctuation dynamo in non-helical, incompressible fluid turbulence. Stochastic flux-freezing is critically important to the mechanism of small-scale turbulent dynamo, because distinct field-lines that are initially separated by inertial-range distances arrive to the same point and resistively merge to produce the net magnetic field. See Eq.(56). Our results and analyses point to essential similarities between the finite-Pr_m and $Pr_m = 0$ dynamo in their Lagrangian mechanisms. Understanding the saturation effect of the Lorentz force from a Lagrangian perspective is an obvious next step. In addition, there will be interesting applications of stochastic flux-freezing to many other problems, e.g. to the theory of fast turbulent reconnection. This will be the subject of future work.

ACKNOWLEDGMENTS

Appendix: Path-Integral Formulas

We here sketch the derivation of the path-integral formulas (9) and (11) in the text. There are discussions already available in the literature [22, 23], but we stress here some connections not found in those works, with rigorous stochastic analysis, on the one hand, and with Feynman path-integral methods, on the other.

Our starting point is the SDE (8), which we discretize using the Euler-Maruyama scheme:

$$\mathbf{X}_n = \mathbf{X}_{n-1} + \mathbf{u}(\mathbf{X}_{n-1}, t_{n-1})\delta t + \sqrt{2\kappa}(\mathbf{W}_n - \mathbf{W}_{n-1}). \tag{A.1}$$

Note that the Brownian-motion variables at the discrete set of times have the Gaussian density (with $\mathbf{W}_0 \equiv \mathbf{0}$)

$$\mathcal{P}(\mathbf{W}_1, ..., \mathbf{W}_N) = (const.) \exp\left(-\frac{1}{2\delta t}\sum_{n=1}^{N}|\mathbf{W}_n - \mathbf{W}_{n-1}|^2\right). \tag{A.2}$$

with respect to $D\mathbf{W} = \prod_n d\mathbf{W}_n$. We can obtain the density $\mathcal{P}(\mathbf{X})$ from the change of variables formula $\mathcal{P}(\mathbf{X}) = \mathcal{P}(\mathbf{W})/\left|\det\left(\frac{\partial\mathbf{X}}{\partial\mathbf{W}}\right)\right|$. It is easy to see from (A.1) that the $(3N) \times (3N)$ Jacobian matrix $\frac{\partial\mathbf{X}}{\partial\mathbf{W}}$ is block lower-triangular, with diagonal blocks $\frac{\partial\mathbf{X}_n}{\partial\mathbf{W}_n} = \sqrt{2\kappa}\mathbf{I}$, for the 3×3 identity matrix $\mathbf{I}$. Thus, $\det\left(\frac{\partial\mathbf{X}}{\partial\mathbf{W}}\right) = const.$ and

$$\mathcal{P}(\mathbf{X}_1, ..., \mathbf{X}_N) \propto \exp\left(-\frac{1}{4\kappa}\sum_{n=1}^{N}\delta t\left|\frac{\mathbf{X}_n - \mathbf{X}_{n-1}}{\delta t} - \mathbf{u}(\mathbf{X}_{n-1}, t_{n-1})\right|^2\right) \tag{A.3}$$

Integrating this density with respect to $D\mathbf{X} = \prod_n d\mathbf{X}_n$ and taking the continuous-time limit $\delta t \to 0, N \to \infty$, one formally obtains formulas like (9) and (11).

The mathematically rigorous versions of these path-integral formulas is the classical *Girsanov transformation* [91], or see Chung and Williams [92] for a modern proof. We shall just remind the reader of this result, in its simplest terms. Suppose that $\mathcal{W}_\kappa$ is a Wiener measure over a rescaled Brownian motion $\sqrt{2\kappa}\mathbf{W}(t)$ and $\mathcal{W}_{1/2} = \mathcal{W}$ is the standard Wiener measure. Suppose that $\mathbf{u}(\mathbf{x}, t)$ is any smooth vector field and $\mathbf{W}(t)$ is defined in terms of $\mathbf{X}(t)$ by integrating (8):

$$\mathbf{W}(t) = \frac{1}{\sqrt{2\kappa}}\left[\mathbf{X}(t) - \mathbf{x}_0 - \int_0^t ds\,\mathbf{u}(\mathbf{X}(s), s)\right].$$

Then Girsanov's theorem states that

$$\mathcal{D}\mathcal{W}_\kappa(\mathbf{X})\exp\left[\frac{1}{2\kappa}\left(\int_0^T \mathbf{u}(\mathbf{X}, t)\cdot d\mathbf{X} - \frac{1}{2}\int_0^T u^2(\mathbf{X}, t)\,dt\right)\right] = \mathcal{D}\mathcal{W}(\mathbf{W}), \tag{A.4}$$

where

$$\int_0^T \mathbf{u}(\mathbf{X}, t)\cdot d\mathbf{X} = \lim_{N\to\infty}\sum_{n=1}^{N}\mathbf{u}(\mathbf{X}_{n-1}, t_{n-1})\cdot(\mathbf{X}_n - \mathbf{X}_{n-1})$$

is the usual Ito stochastic integral [91, 92]. This is easily seen to be equivalent to (A.3) by expanding the square in the exponent of the latter and noting that $D\mathbf{X} \exp\left(-\frac{1}{4\kappa\delta t}\sum_{n=1}^{N}|\mathbf{X}_n - \mathbf{X}_{n-1}|^2\right)$ converges to the Wiener measure $\mathcal{DW}_\kappa(\mathbf{X})$ in the continuum limit.

Although the Euler-Maruyama scheme provides the simplest derivation of such path-integral formulas, other discretizations are possible and yield the same results. E.g., suppose that the trapezoidal rule is employed:

$$\mathbf{X}_n = \mathbf{X}_{n-1} + \frac{\mathbf{u}(\mathbf{X}_n, t_n) + \mathbf{u}(\mathbf{X}_{n-1}, t_{n-1})}{2}\delta t + \sqrt{2\kappa}(\mathbf{W}_n - \mathbf{W}_{n-1}). \quad \text{(A.5)}$$

The sum in the exponent of (A.3) is replaced by

$$\sum_{n=1}^{N}\delta t\left|\frac{\mathbf{X}_n - \mathbf{X}_{n-1}}{\delta t} - \frac{\mathbf{u}(\mathbf{X}_n, t_n) + \mathbf{u}(\mathbf{X}_{n-1}, t_{n-1})}{2}\right|^2.$$

Expanding and taking the continuum limit, this converges formally to

$$\int_0^T |\dot{\mathbf{X}}|^2\, dt - 2\int_0^T \mathbf{u}(\mathbf{X}, t)\circ d\mathbf{X} + \int_0^T u^2(\mathbf{X}, t)\, dt,$$

where

$$\int_0^T \mathbf{u}(\mathbf{X}, t)\circ d\mathbf{X} =$$
$$\lim_{N\to\infty}\sum_{n=1}^{N}\frac{\mathbf{u}(\mathbf{X}_n, t_n) + \mathbf{u}(\mathbf{X}_{n-1}, t_{n-1})}{2}\cdot(\mathbf{X}_n - \mathbf{X}_{n-1})$$
$$\text{(A.6)}$$

is the Stratonovich stochastic integral. Since formally $\mathcal{DQ}_\kappa(\mathbf{X}) = \mathcal{D}\mathbf{X}\exp\left(-\frac{1}{4\kappa}\int_0^T |\dot{\mathbf{X}}|^2\, dt\right)$, it appears that we recover the same result as before but with the Stratonovich integral substituted for the Ito integral in equation (A.4). However, we have not yet computed the contribution of the Jacobian determinant to the change of variables. With the discretization (A.5) the Jacobian matrix $\frac{\partial \mathbf{X}}{\partial \mathbf{W}}$ is block lower-triangular, with diagonal blocks

$$\frac{\partial \mathbf{X}_n}{\partial \mathbf{W}_n} = \sqrt{2\kappa}\left(\mathbf{I} - \frac{1}{2}\delta t\frac{\partial \mathbf{u}}{\partial \mathbf{x}}(\mathbf{X}_n, t_n)\right)^{-1}$$
$$= \sqrt{2\kappa}\exp\left(\frac{1}{2}\delta t\frac{\partial \mathbf{u}}{\partial \mathbf{x}}(\mathbf{X}_n, t_n) + O(\delta t^2)\right).$$

Thus, using $\det(\exp\mathbf{A}) = \exp(\operatorname{tr}\mathbf{A})$,

$$\det\left(\frac{\partial \mathbf{X}}{\partial \mathbf{W}}\right) \propto \exp\left(\frac{1}{2}\sum_{n=1}^{N}\delta t\,(\boldsymbol{\nabla}\cdot\mathbf{u})(\mathbf{X}_n, t_n) + O(\delta t)\right)$$
$$\longrightarrow \exp\left(\frac{1}{2}\int_0^T (\boldsymbol{\nabla}\cdot\mathbf{u})(\mathbf{X}, t)\, dt\right)$$

in the continuum limit $N \to \infty$. The integral in the latter exponent can be expressed in terms of the quadratic variation process [92]

$$\langle X, Y\rangle_T = \lim_{N\to\infty}\sum_{n=1}^{N}(X_n - X_{n-1})(Y_n - Y_{n-1}).$$

Using $d\langle X_i, X_j\rangle_t = 2\kappa\delta_{ij}dt$, one obtains

$$\frac{1}{2}\int_0^T (\boldsymbol{\nabla}\cdot\mathbf{u})(\mathbf{X}, t)\, dt = \frac{1}{4\kappa}\int_0^T d\langle \mathbf{u}(\mathbf{X}, t); \mathbf{X}\rangle.$$

But the standard relation between Ito and Stratonovich integrals,

$$\int_0^T \mathbf{u}(\mathbf{X}, t)\circ d\mathbf{X} - \frac{1}{2}\int_0^T d\langle \mathbf{u}(\mathbf{X}, t); \mathbf{X}\rangle = \int_0^T \mathbf{u}(\mathbf{X}, t)\cdot d\mathbf{X},$$

then recovers (A.4) exactly as before.

For physicists, an illuminating derivation of the path-integral formulas can be based on Feynman's famous formula for the transition amplitude of a quantum, nonrelativistic, charged particle moving in a scalar potential V and in a magnetic field with vector potential $\mathbf{A}$. Feynman's result was

$$\langle \mathbf{x}, t|\mathbf{x}_0, 0\rangle = \int_{\mathbf{x}(0)=\mathbf{x}_0}^{\mathbf{x}(t)=\mathbf{x}} \mathcal{D}\mathbf{x}\exp\left(\frac{i}{\hbar}\int_0^t ds\,\mathcal{L}(s)\right),$$

where $\mathcal{L}(t)$ is the classical Lagrangian

$$\mathcal{L}(t) = \frac{1}{2}m|\dot{\mathbf{x}}|^2 + \frac{e}{c}\mathbf{A}(\mathbf{x}, t)\cdot\dot{\mathbf{x}} - V(\mathbf{x}, t)$$

and the amplitude satisfies the Schrödinger equation

$$i\hbar\partial_t\Psi = \frac{1}{2m}\left(-i\hbar\boldsymbol{\nabla} - \frac{e}{c}\mathbf{A}(\mathbf{x}, t)\right)^2\Psi + V(\mathbf{x}, t)\Psi.$$

See Feynman [93], p.376 or later treatments [94]. Taking imaginary time $T = it$, $\mathbf{u} = i\frac{e\mathbf{A}}{mc}$, $\kappa = \frac{\hbar}{2m}$ and

$$V = -\frac{e^2}{2mc^2}A^2 - i\frac{\hbar e}{2mc}\boldsymbol{\nabla}\cdot\mathbf{A},$$

yields the path-integral formula (9) and converts the Schrödinger equation into the diffusion equation $\partial_T\Psi = \kappa\triangle\Psi - (\mathbf{u}\cdot\boldsymbol{\nabla})\Psi$. This is very straightforward to check in the Coulomb gauge $\boldsymbol{\nabla}\cdot\mathbf{A} = 0$. For a general choice of gauge, note that the vector potential term in the classical action $\mathcal{L}(s)$ yields a term in the exponent of Feynman's path-integral formula which must be interpreted as a Stratonovich integral:

$$\int_0^t \mathbf{A}(\mathbf{x}, s)\cdot\dot{\mathbf{x}}(s)\, ds \equiv \int_0^t \mathbf{A}(\mathbf{x}, s)\circ d\mathbf{x}(s).$$

This is implicit in Feynman's original derivation, who used the midpoint discretization to define the above integral [93]. This point has been carefully discussed elsewhere [94]. If this Stratonovich integral is combined with the $\boldsymbol{\nabla}\cdot\mathbf{A}$ term from the potential, one gets a net contribution to the action proportional to

$$\int_0^T \mathbf{u}(\mathbf{X}, t)\circ d\mathbf{X} + \frac{1}{2}\int_0^T d\langle \mathbf{u}(\mathbf{X}, t); \mathbf{X}\rangle = \int_0^T \mathbf{u}(\mathbf{X}, t)\cdot\widehat{d\mathbf{X}},$$

where now $t = is$ and

$$\int_0^T \mathbf{u}(\mathbf{X}, t) \cdot \widehat{d\mathbf{X}} = \lim_{N \to \infty} \sum_{n=1}^N \mathbf{u}(\mathbf{X}_n, t_n) \cdot (\mathbf{X}_n - \mathbf{X}_{n-1})$$

is the *backward Ito integral.* One obtains a result just like the Girsanov formula (A.4) but with the usual (forward) Ito integral replaced by a backward Ito integral.

Feynman's result is correct. As we stressed in the text, our path-integral formulas (9) and (11) correspond to solving the SDE (8) backward in time, e.g. with the backward Euler-Maruyama scheme

$$\mathbf{X}_{n-1} = \mathbf{X}_n - \mathbf{u}(\mathbf{X}_n, t_n)\delta t + \sqrt{2\kappa}(\mathbf{W}_{n-1} - \mathbf{W}_n) \quad \text{(A.7)}$$

for $t_{n-1} = t_n - \delta t$. If we repeat the steps that led us to (A.3), we now obtain

$$\mathcal{P}(\mathbf{X}_1, ..., \mathbf{X}_N) \propto$$
$$\exp\left(-\frac{1}{4\kappa}\sum_{n=1}^N \delta t \left|\frac{\mathbf{X}_n - \mathbf{X}_{n-1}}{\delta t} - \mathbf{u}(\mathbf{X}_n, t_n)\right|^2\right). \tag{A.8}$$

Integrating this density with respect to $D\mathbf{X} = \prod_n d\mathbf{X}_n$ and taking the continuous-time limit $\delta t \to 0, N \to \infty$, one formally obtains a Girsanov-type formula with the forward Ito integral replaced by a backward Ito integral. This is the rigorous version of our formulas (9) and (11), which correspond exactly to Feynman's old result.

[1] H. Alfvén, Ark. Mat., Astron. o. Fys., **29B**, 1 (1942).
[2] R. Kulsrud, *Plasma Physics for Astrophysics* (Princeton University Press, Princeton, NJ, 2005).
[3] D. Bernard, K. Gawędzki, and A. Kupiainen, J. Stat. Phys., **90**, 519 (1998).
[4] K. Gawędzki and M. Vergassola, Physica D, **138**, 63 (2000).
[5] M. Chaves, K. Gawędzki, P. Horvai, A. Kupiainen, and M. Vergassola, J. Stat. Phys., **113**, 643 (2003).
[6] A. Kupiainen, Ann. Henri Poincaré, **4**, S713 (2003).
[7] W. E and E. Vanden-Eijnden, Proc. Natl. Acad. Sci., **97**, 8200 (2000).
[8] W. E and E. Vanden-Eijnden, Physica D, **152-153**, 636 (2001).
[9] L. F. Richardson, Proc. R. Soc. London, Ser. A, **110**, 709 (1926).
[10] G. L. Eyink and A. F. Neto, New J. Phys., **12**, 023021 (2010).
[11] G. L. Eyink, Phys. Rev. E, **82**, 046314 (2010).
[12] A. P. Kazantsev, Sov. Phys. JETP, **26**, 1031 (1968).
[13] R. H. Kraichnan and S. Nagarajan, Phys. Fluids, **10**, 859 (1967).
[14] R. H. Kraichnan, Phys. Fluids, **11**, 945 (1968).
[15] Y. Li, E. Perlman, M.-P. Wan, Y. Yang, C. Meneveau, R. Burns, S. Chen, A. Szalay, and G. L. Eyink, J. Turbulence, **9**, 31 (2008).
[16] E. Perlman, R. Burns, Y. Li, and C. Meneveau, in *Supercomputing, 2007. SC'07. Proceedings of the ACM/IEEE Conference on Supercomputing (SC07) in Reno, Nevada* (IEEE Xplore, 2007).
[17] N. E. L. Haugen, A. Brandenburg, and W. Dobler, Phys. Rev. E, **70**, 016308 (2004).
[18] A. Schekochihin, S. C. Cowley, S. Taylor, J. Maron, and J. C. McWilliams, Astrophys. J., **612**, 276 (2004).
[19] G. Eyink and J. Xin, J. Stat. Phys., **100**, 679 (2000).
[20] A. M. Obukhov, Izv. Akad. Nauk SSSR, Ser. Geogr. Geoz., **5**, 453 (1941).
[21] P. Hartman, *Ordinary Differential Equations*, 2nd ed. (SIAM, 2002).
[22] I. T. Drummond, J. Fluid Mech., **123**, 59 (1982).
[23] B. I. Shraiman and E. D. Siggia, Phys. Rev. E, **49**, 2912 (1994).
[24] G. Paladin and A. Vulpiani, Phys. Rep., **156**, 147 (1987).
[25] G. K. Batchelor, Q. J. R. Meteorol. Soc., **76**, 133 (1950).
[26] G. K. Batchelor, Proc. Camb. Phil. Soc., **48**, 345 (1952).
[27] R. H. Kraichnan, Phys. Fluids, **9**, 1937 (1966).
[28] B. L. Sawford, P. K. Yeung, and M. S. Borgas, Phys. Fluids, **17**, 095109 (2005).
[29] S. Ott and J. Mann, J. Fluid Mech., **422**, 207 (2000).
[30] M. Bourgoin, N. T. Ouellette, H. Xu, J. Berg, and E. Bodenschatz, Science, **311**, 835 (2006).
[31] N. T. Ouellette, H. Xu, M. Bourgoin, and E. Bodenschatz, New J. Phys., **8**, 109 (2006).
[32] H. Xu, N. T. Ouellette, and E. Bodenschatz, New J. Phys., **10**, 013012 (2008).
[33] T. Ishihara and Y. Kaneda, Phys. Fluids, **14**, L69 (2002).
[34] L. Biferale, G. Boffetta, A. Celani, B. J. Devenish, A. Lanotte, and F. Toschi, Phys. Fluids, **17**, 115101 (2005).
[35] B. L. Sawford, P. K. Yeung, and J. F. Hackl, Phys. Fluids, **20**, 065111 (2008).
[36] P. E. Kloeden and E. Platen, *Numerical Solution of Stochastic Differential Equations* (Springer-Verlag, Berlin, 1992).
[37] P. Franzese and M. Cassiani, J. Fluid Mech., **571**, 391 (2007).
[38] We take this opportunity to correct a typo in our previous paper [45] where it was incorrectly written that $\mathbf{u}_e = \mathbf{u} - \frac{m_e c}{4\pi e \rho}\boldsymbol{\nabla}\times\mathbf{B}$, with ρ the mass density and m_e the electron mass. Instead the latter should have been m_i the ion mass.
[39] A. Boozer, Phys. Fluids B, **2**, 2300 (1990).
[40] E. R. Priest, G. Hornig, and D. I. Pontin, J. Geophys. Res., **108**, 1285 (2003).
[41] G. Hornig and E. Priest, Phys. Plasmas, **10**, 2712 (2003).
[42] A. L. Wilmot-Smith, E. R. Priest, and G. Hornig, Geophys. Astrophys. Fluid Dyn., **99**, 177 (2005).
[43] I. T. Molchanov, A. A. Ruzmaikin, and D. D. Sokoloff, Geophys. Astrophys. Fluid Dyn., **30**, 241 (1984).
[44] I. T. Drummond and R. R. Horgan, J. Fluid Mech., **163**, 425 (1986).
[45] G. L. Eyink, J. Math. Phys., **50**, 083102 (2009).
[46] S. Lundquist, Phys. Rev., **83**, 307 (1951).
[47] This interpretation requires some caution. The quantity

$$\tilde{\rho}(\mathbf{x}, t) \equiv \left.\frac{\rho_0(\mathbf{a})}{\det(\boldsymbol{\nabla}_a \tilde{\mathbf{x}}(\mathbf{a}, t))}\right|_{\tilde{\mathbf{a}}(\mathbf{x}, t)}$$

satisfies the stochastic (Stratonovich) equation

$$\partial_t \tilde{\rho}(\mathbf{x}, t) + \boldsymbol{\nabla} \cdot \left[\left(\mathbf{u}(\mathbf{x}, t) + \sqrt{2\lambda} \tilde{\boldsymbol{\eta}}(t) \right) \circ \tilde{\rho}(\mathbf{x}, t) \right] = 0$$

with initial condition $\tilde{\rho}(\mathbf{x}, t_0) = \rho_0(\mathbf{x})$. It thus represents the mass density in the random flow with noise realization $\tilde{\eta}(t)$. However, the noise-average $\bar{\rho}(\mathbf{x}, t) \equiv \overline{\tilde{\rho}(\mathbf{x}, t)}$ is *not* the physical mass density! In fact, by converting the previous stochastic equation to Ito form and taking the average, it follows that

$$\partial_t \bar{\rho}(\mathbf{x}, t) + \boldsymbol{\nabla} \cdot (\mathbf{u}(\mathbf{x}, t) \bar{\rho}(\mathbf{x}, t)) = \lambda \triangle \bar{\rho}(\mathbf{x}, t),$$

which is not the correct continuity equation.

[48] E. Villermaux and Y. Gagne, Phys. Rev. Lett., **73**, 252 (1994).

[49] F. Nicolleau and A. Elmaihy, J. Fluid Mech., **517**, 229 (2004).

[50] L. C. Young, Acta Math., **67**, 251 (1936).

[51] G. L. Eyink, Phys. Lett. A, **368**, 486 (2007).

[52] Note that the addition of loops is pointwise. That is, if two loops C, C' are given parametrically by periodic functions $C, C' : s \in [0, 1] \mapsto C(s), C'(s) \in \mathbb{R}^3$, then the sum-loop $C + C'$ is parameterized by $(C + C')(s) = C(s) + C'(s)$..

[53] S. I. Braginski, Rev. Plasma Phys., **1**, 205 (1965).

[54] E. G. Zweibel and M. Yamada, Annu. Rev. Astron. Astrophys., **47**, 291 (2009).

[55] H. K. Moffatt, J. Fluid Mech., **65**, 1 (1974).

[56] R. H. Kraichnan, J. Fluid Mech., **75**, 657 (1976).

[57] R. H. Kraichnan, J. Fluid Mech., **77**, 753 (1976).

[58] S. I. Vainshtein and L. L. Kichatinov, J. Fluid Mech., **168**, 73 (1986).

[59] L. L. Kichatinov, J. Fluid Mech., **208**, 115 (1989).

[60] J. Cho, E. T. Vishniac, A. Beresnyak, A. Lazarian, and D. Ryu, Astrophys. J., **693**, 1449 (2009).

[61] J. Cho and D. Ryu, Astrophys. J., **705**, L90 (2009).

[62] I. Lerche, J. Math. Phys., **14**, 1381 (1973).

[63] The important papers of Vainshtein and Kichatinov [58, 59] employ a representation in terms of 2-particle turbulent diffusion, but this is a technical device to avoid the direct appearance of space-gradients. We might note also that these these authors believed that for $\eta = 0$ the transition probability $p_2(\mathbf{x}, {}^1\mathbf{x} | \mathbf{z}, {}^1\mathbf{z}, t)$ of two fluid particles should be "going to zero when $\mathbf{z} = {}^1\mathbf{z}$ and $\mathbf{x} \neq {}^1\mathbf{x}$". They thus miss the phenomenon of spontaneous stochasticity. They furthermore wrote on turbulent dynamo at high Reynolds numbers that: "For the magnetic field, there also exists a region of scales in which $R_m \gg 1$, i.e. the frozen-in condition is fulfilled". Their paper thus provides another example in which flux-freezing is assumed to hold, incorrectly, for Reynolds numbers $Re, Re_m \gg 1$..

[64] G. L. Eyink, Phys. Fluids, **20**, 125101 (2008).

[65] This quantity was previously [10] denoted $\bar{F}_{k\ell}^{ij}(\mathbf{a}, \mathbf{a}', t_0 | \mathbf{x}, \mathbf{x}', t)$..

[66] J. Cho and E. T. Vishniac, Astrophys. J., **538**, 217 (2000).

[67] W. Hoeffding, *The strong law of large numbers for U-statistics*, Mimeo Series 302 (Institute of Statistics, Univ. of North Carolina, Chapel Hill, NC, 1961).

[68] R. J. Serfling, *Approximation Theorems of Mathematical Statistics* (John Wiley, New York, 1980).

[69] There was one additional complication in the calculation. As a modest requirement for accuracy, we required that the magnetic energy at each of the 1600 points $\mathbf{x}_s$ should be positive and with relative error less than 50% for times $t = t_f - \tau$ less than $10t_\eta$. This criterion was easily satisfied for most points, with $N = 1024$ particles. However, there were 7 points of the 1600 for which this number N did not suffice. These were points of very large magnitude of velocity-gradient, two or three times the rms value, associated to turbulent intermittency. For such points, we had to use more particles, up to $N = 65,536$ or more than 2 billion particle-pairs in the worst case.

[70] This Green's function was denoted in our previous work [10] as $\bar{F}$ and F was used for the corresponding adjoint Green's function.

[71] D. Vincenzi, J. Stat. Phys., **106**, 1073 (2002).

[72] P. Goldreich and S. Sridhar, Astrophys. J., **438**, 763 (1995).

[73] P. Goldreich and S. Sridhar, Astrophys. J., **485**, 680 (1997).

[74] S. Galtier, S. V. Nazarenko, A. C. Newell, and A. Pouquet, J. Plasma Phys., **63**, 447 (2000).

[75] A. Balk, J. Fluid Mech., **467**, 163 (2002).

[76] A. Busse and W.-C. Müller, Astron. Nachr., **329**, 714 (2008).

[77] W.-C. Müller and A. Busse, Europhys. Lett., **78**, 14003 (2007).

[78] A. Busse, W.-C. Müller, H. Homann, and R. Grauer, Phys. Plasmas, **14**, 122303 (2007).

[79] Recall that in GS theory, the mean energy dissipation for sub-Alfvénic turbulence scales as $\varepsilon \sim (u')^4 / v_A L_u$. Using this relation, (57) becomes $r_\perp^2(t) \sim L_i^2 (u'/v_A)(t/T_u)^3$ and (58) becomes $r_\parallel^2(t) \sim L_i^2 (u'/v_A)^4 (t/T_u)^4$. Since $u' \leq v_A$, these formulas imply that $r_\parallel(t) \ll r_\perp(t)$ for $t \ll T_u$..

[80] A. Beresnyak and A. Lazarian, Astrophys. J., **640**, L175 (2006).

[81] J. Mason, F. Cattaneo, and S. Boldyrev, Phys. Rev. Lett., **97**, 255002 (2006).

[82] J. D. Bekenstein and A. Oron, Phys. Rev. E, **62**, 5594 (2000).

[83] E. A. Kuznetsov and V. P. Ruban, Phys. Rev. E., **61**, 831 (2000).

[84] A. Lazarian and E. Vishniac, Astrophys. J., **517**, 700 (1999).

[85] E. N. Parker, Astrophys. J., **401**, 137 (1992).

[86] D. Galloway, "Fast dynamos," in *Advances in Nonlinear Dynamos*, edited by A. Ferriz-Mas and M. Nunez (CRC Press, 2003) Chap. 2, pp. 37–59.

[87] G. L. Eyink and H. Aluie, Physica D, **223**, 82 (2006).

[88] L. Onsager, Nuovo Cim. Suppl., **6**, 279 (1949).

[89] G. Eyink, Physica D, **237**, 1956 (2008).

[90] G. L. Eyink, Physica D, **239**, 1236 (2010).

[91] I. V. Girsanov, Theory Probab. Appl., **5**, 285 (1960).

[92] K. L. Chung and R. J. Williams, *Introduction to Stochastic Integration* (Birkhäuser, Boston, 1990).

[93] R. P. Feynman, Rev. Mod. Phys., **20**, 367 (1948).

[94] B. Gaveau, E. Mihóková, M. Roncadelli, and L. S. Schulman, Am. J. Phys., **72**, 385 (2004).